Gen Thorac Cardiovasc Surg (2014) 62:157–162
DOI 10.1007/s11748-013-0345-y

ORIGINAL ARTICLE

FDG PET/CT is useful for detecting infiltration to the port site in patients with malignant pleural mesothelioma

Koji Kawaguchi · Tetsuo Taniguchi · Noriyasu Usami · Takayuki Fukui · Futoshi Ishiguro · Shota Nakamura · Kohei Yokoi

Received: 4 September 2013 / Accepted: 3 November 2013 / Published online: 27 November 2013

Abstract
Objective One reason for the poor outcomes of multimodality therapies, including macroscopic complete resection, in patients with malignant pleural mesothelioma (MPM) is the difficulty of correctly staging the disease, which can result in incomplete resection. The purpose of this study was to investigate the aspects of tumor infiltration to the port site and the usefulness of preoperative FDG PET/CT for diagnosing MPM.
Methods Between June 2007 and May 2013, 21 patients who underwent surgical treatment with curative intent for MPM that had been previously diagnosed on a video-assisted thoracic surgery (VATS) biopsy were included in this study.
Results There were 17 males and four females, with a mean age of 63 years. The accumulation of FDG at the port site was observed in all nine patients with tumor infiltration to the port site, whereas this feature was not noted in 15 patients without tumor extension to the port site. There were more positive lymph node cases in the infiltration group than in the non-infiltration group ($p = 0.02$). No significant differences in survival were observed between the patients with and without tumor infiltration to the port site.
Conclusions FDG PET/CT is useful for detecting tumor infiltration of MPM to the port site and may help to prevent local recurrence, especially port site relapse, following macroscopic complete resection. However, this condition is related to tumor aggressiveness; therefore, performing careful staging and determining the appropriate treatment strategy are required in such patients.

Keywords Malignant pleural mesothelioma · Port site infiltration · FDG PET/CT · Staging

K. Kawaguchi (✉) · T. Taniguchi · N. Usami · T. Fukui · F. Ishiguro · S. Nakamura · K. Yokoi
Department of Thoracic Surgery, Nagoya University Graduate School of Medicine, 65 Tsurumai-cho, Showa-ku, Nagoya 466-8550, Japan
e-mail: gucci@med.nagoya-u.ac.jp

Introduction

The surgical outcomes of extrapleural pneumonectomy (EPP) for malignant pleural mesothelioma (MPM) are far from satisfactory [1]. One reason for the poor outcomes is the difficulty of correctly staging the disease, which can result in incomplete resection [2].

Tumor extension to port sites created for the purpose of performing biopsies of tumors or drainage of pleural effusion has been reported to be a poor prognostic factor [3, 4]. Therefore, thoracic surgeons must excise all port sites with the specimens. However, it is difficult to confirm whether the tumor has infiltrated to the port site or only fibrous changes are present during surgery, which may result in a positive surgical margin at the port site [5]. If preliminary findings of tumor infiltration at the port site could be accurately obtained, then the ability to perform selective excision of port sites with an adequate margin would thus be expected to reduce the incidence of pathological positive surgical margins and local relapse.

The purpose of this study was to investigate the aspects of tumor infiltration to the port site and the usefulness of preoperative [18F]-fluorodeoxyglucose positron emission tomography (FDG PET)/computed tomography (CT) for diagnosing MPM.

Patients and methods

Between June 2007 and May 2013, 21 patients underwent surgical treatment with curative intent for MPM that had been pathologically diagnosed using a video-assisted thoracic surgery (VATS) biopsy. Surgical cases in which the diagnosis of MPM was made based on the findings of a needle biopsy, and those in which macroscopic complete resection was not accomplished were excluded from this study. Patient characteristics and clinical information were collected from the hospital database, and the study was approved by the Institutional Review Board of Nagoya University Hospital. We evaluated the perioperative findings and prognoses of the MPM patients with tumor infiltration to the port site, which represents an extension of the tumor into the soft tissue of the chest wall around the port site.

Regarding preoperative staging procedures, all patients routinely underwent thin-slice contrast-enhanced CT and FDG PET/CT. These examinations were performed at both pre- and post-neoadjuvant chemotherapy when patients received it. The details of the FDG PET/CT scanners are the same as those described previously for evaluating thymic epithelial tumors [6]. In brief, the patients received an intravenous injection of 3.7–4.07 MBq/kg of FDG. Image acquisition was performed using a PET/CT scanner (Biograph16; Siemens Medical Solutions, Erlangen, Germany). The emission PET images were reconstructed using iterative ordered subset expectation maximization with non-contrast CT. For the semiquantitative assessment, regions of interest (ROIs) were overlaid on FDG-avid tumors, and the SUVmax [the maximum ROI activity (MBq/g)/injected dose (MBq)/body weight (g)] of each tumor was measured. The positive accumulation of FDG was defined as a SUVmax value >2.0 [7].

The staging system of the International Mesothelioma Interest Group (IMIG) for MPM was adopted in this study [8]. Tumor infiltration to the port site is staged as T3 in this system. The clinical staging was determined based on the radiological findings and the indications for the surgical procedures were judged carefully by multidisciplinary physicians. Regarding the preoperative evaluations of lymph node metastasis on FDG PET/CT, findings of a short diameter of the lymph node >1 cm and FDG accumulation were considered to be signs of lymph node metastasis.

Our surgical treatment for MPM has changed during the study period. After the results of the MARS trial [9] were published, a feasibility study of pleurectomy/decortication (P/D) after neoadjuvant chemotherapy for resectable MPM was conducted in Japan. Our institution participated in this study and adopted the surgical method of P/D, especially in patients with an advanced stage of MPM. All patients underwent diaphragmatic resection and en bloc excision of each port site from the skin, chest wall (muscles and fat tissue, without ribs) and uninterrupted to the parietal pleura in addition to EPP or P/D (Fig. 2). Reconstruction of the diaphragm and pericardium was performed using Goretex® patches (2 and 0.1 mm, respectively), if necessary. Neoadjuvant chemotherapy was usually administered and consisted of three courses of cisplatin and pemetrexed. Patients who underwent EPP were recommended to receive 54 Gy of postoperative radiotherapy for hemithorax approximately 2 months after the surgery. When the presence of tumor infiltration to the port site was proven on a pathologic examination, the administration of additional dose (usually 10 Gy/5 Fr) of radiation to the area was recommended.

Comparisons of the preoperative findings were made using the Chi Square test. The survival time was measured from the date of surgery to the date of death or the last follow-up. Survival curves were estimated according to the Kaplan–Meier method, and differences in survival were assessed using the log-rank test. A p value of <0.05 was considered to be significant. The data were analyzed using the SPSS 20.0 software program (SPSS, Inc., Chicago, IL, USA).

Table 1 Characteristics of the patients who underwent macroscopic complete resection for malignant pleural mesothelioma

Variable	Number of patients	%
Mean age (range)	63 (46–72)	
Gender		
Male	17	81
Female	4	19
Histology		
Epithelioid	16	76
Biphasic	5	24
Surgical procedure		
Extrapleural pneumonectomy	17	81
Extended pleurectomy/decortication	4	19
pN status		
N0	13	62
N1	2	9
N2	6	29
Induction chemotherapy		
Yes	15	71
No	6	29
Adjuvant therapy		
CT + RT	3	14
RT	9	43
CT	1	5
None	8	38

CT chemotherapy, *RT* radiotherapy

Table 2 Comparison of the patients with and without tumor infiltration at the port site

Variable	Positive	Negative	*p*
Gender			0.149
Male	6	11	
Female	3	1	
Chest pain			0.697
Yes	3	5	
No	6	7	
Number of the ports at VATS biopsy			0.062
Mean	2.1	1.2	
Range	1–3	1–2	
Accumulation of FDG at the port sites on PET/CT			<0.001
Positive	9	0	
Negative	0	12	
Histology			0.882
Epithelioid	7	9	
Biphasic	2	3	
Lymph node metastasis			0.020
Positive	6	2	
Negative	3	10	

Results

The characteristics of the 21 patients are shown in Table 1. There were 17 males and four females, with a mean age of 63 years. The epithelial subtype was most frequent, followed by the biphasic subtype. Preoperative FDG PET/CT for the purpose of staging or restaging following the administration of neoadjuvant therapy was performed approximately 17 days before the surgical treatment. A total of nine patients were found to have positive accumulation of FDG at the port site. Macroscopic complete resection with excision of all port sites was performed in all patients. Postoperative radiotherapy was administered in 12 patients with EPP, five of whom received additional radiation to port sites with proven tumor infiltration. On the other hand, only one patient who underwent P/D received postoperative radiotherapy to the site of the superior vena cava where the tumor was exposed during surgery.

Table 2 shows the correlations between the patients with and without tumor infiltration to the port site according to various perioperative factors. Three (75 %) of the four females with MPM exhibited tumor infiltration to the port site, while positive infiltration was observed in six (35 %) of 17 male patients ($p = 0.149$). The histological subtype had no relationship to the presence of infiltration at the port site. The number of port sites used for biopsies was greater in the patients with tumor infiltration. The accumulation of FDG at the port site was observed in all nine patients with positive infiltration; however, this feature was not detected in the 12 patients with negative infiltration. In addition, there were more positive lymph node cases in the infiltration group than in the non-infiltration group.

Figure 1 shows the preoperative PET/CT and CT findings of three patients with tumor infiltration of the port site. Neither radiologists nor thoracic surgeons were able to detect tumor infiltration to the port site on contrast-enhanced CT and/or with palpation; such cases were strongly suspected of involving infiltration on PET/CT only. All port sites were excised en bloc with the specimen in spite of the PET/CT and CT findings, and the pathologic results of them were carefully compared with the accumulation of FDG on preoperative PET/CT. Thirteen of 33 excised port sites were proven to be infiltrated with MPM, and 11 port sites were found to exhibit accumulation of FDG; the mean SUVmax was 3.8 (2.0–6.9). Five of the nine patients with positive port sites were proven to have positive surgical margins, although the surgeons tended to excise the port sites with an 'adequate' margin (Fig. 2).

The median follow-up period was 9 months. Eight patients died of recurrent disease. The median survival and two-year survival rate were 37 months and 54 %, respectively. The survival curves of the patients with and without tumor infiltration to the port site are presented in Fig. 3. There were no significant differences in survival between the two groups.

Discussion

Although multimodality therapies, including macroscopic complete resection, are administered in patients with MPM, the prognosis of the disease remains dismal [1, 5]. One reason for the poor outcomes is the difficulty of correctly staging the disease, which can result in incomplete resection [2]. In addition, it is impossible to excise the tumor with an adequately safe margin based on anatomical characteristics, that is, the pleura is not a parenchymatous organ and is widely adjacent to vital structures.

It is well known that MPM easily infiltrates to port sites created for the purpose of performing biopsies of tumors or drainage of pleural effusion [3, 4]. The incidence of port site infiltration in this study was 43 % (nine of 21 patients), while that observed in patients with stage III MPM reported by Bolukbas and coworkers was up to 69 % [3]. Therefore, thoracic surgeons must excise all port sites during surgical resection; however, it is difficult to confirm whether the tumor has infiltrated to the port site or only fibrous changes are present during surgery [10]. As a result, in our study, five of the nine patients with tumor infiltration had a positive surgical margin at the port site. If preliminary findings of tumor infiltration at the port site could

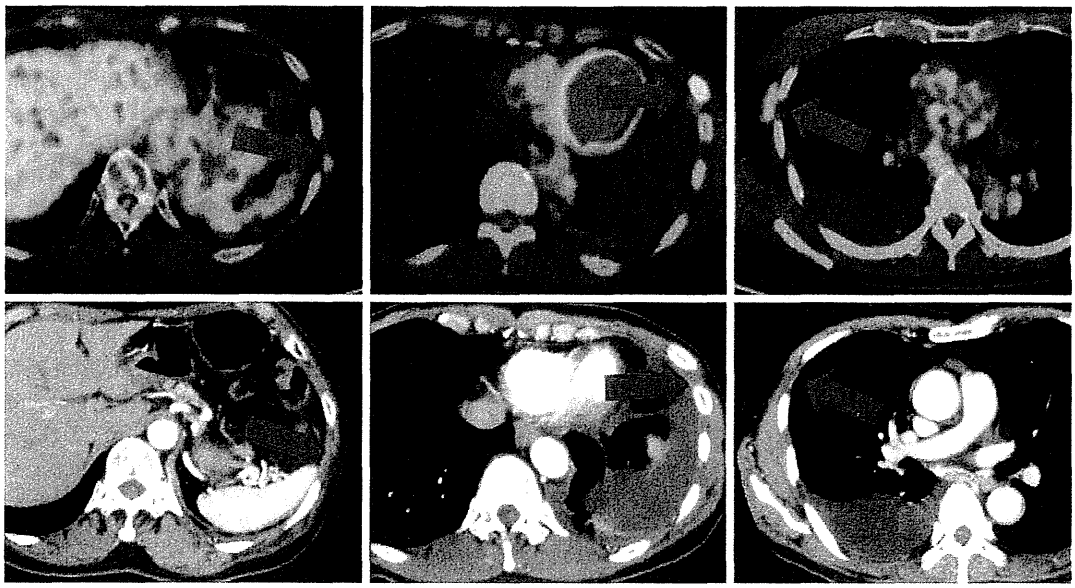

Fig. 1 Preoperative PET/CT and CT findings of three patients with infiltration of malignant pleural mesothelioma (MPM) to the port site. Contrast-enhanced CT revealed no abnormal findings at the port sites, whereas the accumulation of FDG was clearly demonstrated on PET/CT in each case (*arrow*). Pathologic examinations revealed tumor infiltration to the port site in all cases. *Left column* 70-year-old female with the epithelioid subtype. *Middle* 60-year-old female with the epithelioid subtype. *Right* 67-year-old male with the epithelioid subtype

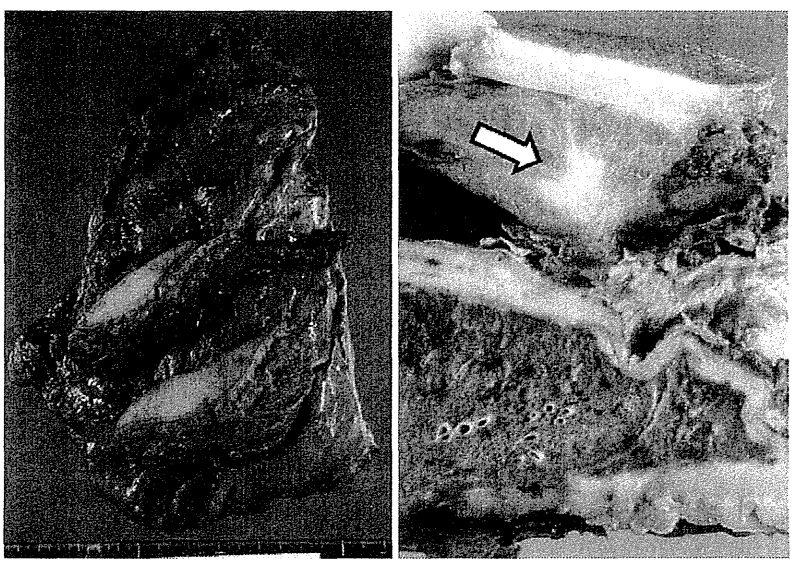

Fig. 2 Resected specimens with the skin and chest wall of the port sites. *Left* A specimen obtained via extrapleural pneumonectomy in concordance with the port site. *Right* A tumor infiltrating to the extrathoracic serratus anterior muscle of the port site (*arrow*)

be accurately diagnosed using PET/CT, the ability to perform selective excision of port sites with adequate margin would decrease the incidence of pathological positive surgical margins and perhaps local relapse.

PET/CT is a useful tool for diagnosis, staging and conducting assessments of the efficacy of chemotherapy in patients with malignant diseases, including MPM. However, the sensitivity and specificity for intrathoracic staging of MPM are relatively low [2, 11–13]. In this study, findings of tumor infiltration at the port site were detected on PET/CT with high accuracy. This is because the port sites were located outside of the thoracic cavity, where the effects of respiratory motion or inflammatory pleuritis are low.

As it is difficult to diagnose MPM based on the results of cytological examinations of pleural effusion only, biopsies of the tumor or pleura using VATS are usually performed. In this study, the mean number of ports used for VATS biopsies in the 12 patients without tumor infiltration was only 1.2; therefore, the use of a lower number of ports may

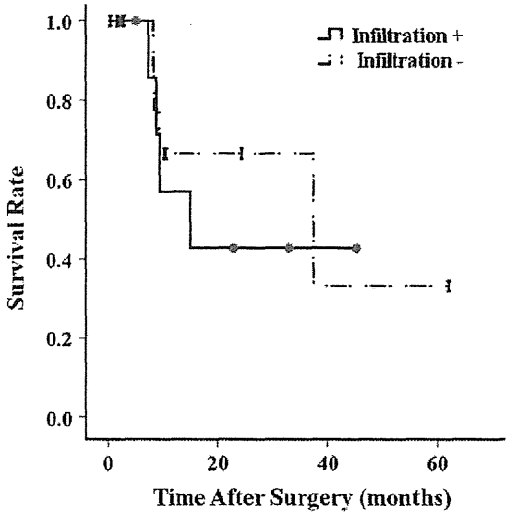

Fig. 3 Survival curves of the patients with and without tumor infiltration to the port site. There were no significant differences in survival between the two groups ($p = 0.934$)

be associated with the prevention of tumor extension into such areas.

There were no significant differences in survival between the patients with and those without tumor infiltration to the port site in this study, in contrast to the findings of previous reports [3, 4]. Possible reasons for this discrepancy include the effectiveness of additional radiation to the port site and the short follow-up period. Nevertheless, the use of local therapies, including excision and radiation, is fundamental for overcoming MPM, as the disease exhibits a predilection for local progression rather than distant metastasis.

There were more cases of positive lymph node metastasis in the patients with tumor infiltration, which may reflect tumor aggressiveness or malignant characteristics. Because the sensitivity and specificity for detecting mediastinal lymph node metastasis using PET/CT and CT are extremely low in patients with MPM based on the findings of previous reports and this study (data not shown), performing additional histological examinations, such as mediastinoscopy or endobronchial ultrasound bronchoscopy, to evaluate the mediastinal lymph nodes is recommended in patients with aggressive disease [2, 14].

In conclusion, FDG PET/CT is useful for detecting tumor infiltration of MPM to the port site and may help to prevent local recurrence, especially port site relapse, after macroscopic complete resection. However, this condition is related to tumor aggressiveness; therefore, performing careful staging and determining the appropriate treatment strategy which sometimes includes non-surgical therapy is required in such patients.

Acknowledgments The authors wish to thank Takashi Nihashi and Katsuhiko Kato (Department of Radiology, Nagoya University Graduate School of Medicine) for their contribution to the measurement of SUVmax in each tumor.

Conflict of interest The authors have declared that no conflict of interest exists.

References

1. Rusch VW, Giroux D, Kennedy C, Ruffini E, Cangir AK, Rice D, et al. Initial analysis of the international association for the study of lung cancer mesothelioma database. J Thorac Oncol. 2012;7:1631–9.
2. Flores RM, Akhurst T, Gonen M, Larson SM, Rusch VW. Positron emission tomography defines metastatic disease but not locoregional disease in patients with malignant pleural mesothelioma. J Thorac Cardiovasc Surg. 2003;126:11–6.
3. Bolukbas S, Eberlein M, Kudelin N, Demes M, Stallmann S, Fisseler-Eckhoff A, et al. Factors predicting poor survival after lung-sparing radical pleurectomy of IMIG stage III malignant pleural mesothelioma. Eur J Cardiothorac Surg. 2013;44:119–23.
4. Richards WG, Godleski JJ, Yeap BY, Corson JM, Chirieac LR, Zellos L, et al. Proposed adjustments to pathologic staging of epithelial malignant pleural mesothelioma based on analysis of 354 cases. Cancer. 2010;116:1510–7.
5. Krug LM, Pass HI, Rusch VW, Kindler HL, Sugarbaker DJ, Rosenzweig KE, et al. Multicenter phase II trial of neoadjuvant pemetrexed plus cisplatin followed by extrapleural pneumonectomy and radiation for malignant pleural mesothelioma. J Clin Oncol. 2009;27:3007–13.
6. Fukumoto K, Taniguchi T, Ishikawa Y, Kawaguchi K, Fukui T, Kato K, et al. The utility of [18F]-fluorodeoxyglucose positron emission tomography-computed tomography in thymic epithelial tumours. Eur J Cardiothorac Surg. 2012;42:e152–6.
7. Benard F, Sterman D, Smith RJ, Kaiser LR, Albelda SM, Alavi A. Metabolic imaging of malignant pleural mesothelioma with fluorodeoxyglucose positron emission tomography. Chest. 1998;114:713–22.
8. Rusch VW. A proposed new international TNM staging system for malignant pleural mesothelioma. From the International Mesothelioma Interest Group. Chest. 1995;108:1122–8.
9. Treasure T, Lang-Lazdunski L, Waller D, Bliss JM, Tan C, Entwisle J, et al. Extra-pleural pneumonectomy versus no extra-pleural pneumonectomy for patients with malignant pleural mesothelioma: clinical outcomes of the Mesothelioma and Radical Surgery (MARS) randomised feasibility study. Lancet Oncol. 2011;12:763–72.
10. Husain AN, Colby T, Ordonez N, Krausz T, Attanoos R, Beasley MB, et al. Guidelines for pathologic diagnosis of malignant mesothelioma: 2012 update of the consensus statement from the International Mesothelioma Interest Group. Arch Pathol Lab Med. 2013;137:647–67.
11. Pilling J, Dartnell JA, Lang-Lazdunski L. Integrated positron emission tomography-computed tomography does not accurately stage intrathoracic disease of patients undergoing trimodality therapy for malignant pleural mesothelioma. Thorac Cardiovasc Surg. 2010;58:215–9.
12. Gerbaudo VH, Sugarbaker DJ, Britz-Cunningham S, Di Carli MF, Mauceri C, Treves ST. Assessment of malignant pleural mesothelioma with (18)F-FDG dual-head gamma-camera coincidence imaging: comparison with histopathology. J Nucl Med. 2002;43:1144–9.

13. Erasmus JJ, Truong MT, Smythe WR, Munden RF, Marom EM, Rice DC, et al. Integrated computed tomography-positron emission tomography in patients with potentially resectable malignant pleural mesothelioma: staging implications. J Thorac Cardiovasc Surg. 2005;129:1364–70.
14. Schaefer NG, Veit-Haibach P, Soyka JD, Steinert HC, Stahel RA. Continued pemetrexed and platin-based chemotherapy in patients with malignant pleural mesothelioma (MPM): value of 18F-FDG-PET/CT. Eur J Radiol. 2012;81:e19–25.

OPEN ACCESS

ORIGINAL ARTICLE

Increased ectodomain shedding of lung epithelial cell adhesion molecule 1 as a cause of increased alveolar cell apoptosis in emphysema

Takahiro Mimae,[1,2] Man Hagiyama,[3] Takao Inoue,[3] Azusa Yoneshige,[3] Takashi Kato,[3] Morihito Okada,[1] Yoshinori Murakami,[2] Akihiko Ito[3]

▶ Additional material is published online only. To view please visit the journal online (http://dx.doi.org/10.1136/thoraxjnl-2013-203867).

[1]Department of Surgical Oncology, Research Institute for Radiation Biology and Medicine, Graduate School of Biomedical Sciences, Hiroshima University, Hiroshima, Japan
[2]Division of Molecular Pathology, Department of Cancer Biology, Institute of Medical Science, University of Tokyo, Tokyo, Japan
[3]Department of Pathology, Faculty of Medicine, Kinki University, Osaka, Japan

Correspondence to
Dr A Ito, Department of Pathology, Faculty of Medicine, Kinki University, 377-2 Ohno-Higashi, Osaka-Sayama, Osaka 589-8511, Japan;
aito@med.kindai.ac.jp

TM and MH contributed equally to this work.

Received 15 May 2013
Revised 22 August 2013
Accepted 11 September 2013
Published Online First
3 October 2013

ABSTRACT

Rationale Alveolar epithelial cell apoptosis and protease/antiprotease imbalance based proteolysis play central roles in the pathogenesis of pulmonary emphysema but molecular mechanisms underlying these two events are not yet clearly understood. Cell adhesion molecule 1 (CADM1) is a lung epithelial cell adhesion molecule in the immunoglobulin superfamily. It generates two membrane associated C terminal fragments (CTFs), αCTF and βCTF, through protease mediated ectodomain shedding.

Objective To explore the hypothesis that more CADM1-CTFs are generated in emphysematous lungs through enhanced ectodomain shedding, and cause increased apoptosis of alveolar epithelial cells.

Methods and results Western blot analyses revealed that CADM1-CTFs increased in human emphysematous lungs in association with increased ectodomain shedding. Increased apoptosis of alveolar epithelial cells in emphysematous lungs was confirmed by terminal nucleotide nick end labelling (TUNEL) assays. NCI-H441 lung epithelial cells expressing mature CADM1 but not CTFs were induced to express αCTF both endogenously (by shedding inducers phorbol ester and trypsin) and exogenously (by transfection). Cell fractionation, immunofluorescence, mitochondrial membrane potentiometric JC-1 dye labelling and TUNEL assays revealed that CADM1-αCTF was localised to mitochondria where it decreased mitochondrial membrane potential and increased cell apoptosis. A mutation in the intracytoplasmic domain abrogated all three abilities of αCTF.

Conclusions CADM1 ectodomain shedding appeared to cause alveolar cell apoptosis in emphysematous lungs by producing αCTF that accumulated in mitochondria. These data link proteolysis to apoptosis, which are two landmark events in emphysema.

Key messages

What is the key question?

▶ Increased alveolar epithelial cell apoptosis and protease/antiprotease imbalance based proteolysis are two landmarks in the pathogenesis of pulmonary emphysema. What mechanisms may underlie these two events?

What is the bottom line?

▶ Lung epithelial cell adhesion molecule 1 (CADM1) generates two membrane associated C terminal fragments (CTFs), αCTF and βCTF, through protease mediated ectodomain shedding. CADM1-αCTF were increased in human emphysematous lungs, and appeared to cause alveolar epithelial cell apoptosis by localising to mitochondria and decreasing mitochondrial membrane potential.

Why read on?

▶ This study identifies CADM1-αCTF as a key molecule responsible for linking between proteolysis and apoptosis in emphysematous lungs, and will aid the development of a target based therapeutic strategy for emphysema.

INTRODUCTION

Emphysema is a pulmonary disease characterised by alveolar wall destruction, resulting in enlarged airspaces and loss of surface area for gas exchange without fibrosis.[1] This unique aspect of alveolar destruction has long been ascribed mainly to excessive apoptosis of alveolar structural (non-inflammatory) cells (ie, epithelial and endothelial cells), and a relative excess of proteases creating a local imbalance between proteases and antiproteases.[2 3] Apoptosis of endothelial cells in the alveolar wall is well explained by two mechanisms: decreased maintenance signals for endothelial cells mediated through vascular endothelial growth factor and its cognate receptor, and increased proteolysis of extracellular matrices in the alveolar wall resulting from a protease/antiprotease imbalance.[3 4] However, the molecular basis for alveolar epithelial cell apoptosis specific to emphysema is not yet fully understood. Involvement of a protease/antiprotease imbalance has generally been speculated because degradation of the extracellular matrix caused by excessive proteases forces alveolar cells to fall into anoikis, a type of programmed cell death, secondary to cell detachment from the matrix.[4] However, studies over the past decade have suggested that alveolar epithelial destruction in emphysematous lungs might occur due to apoptosis, possibly unrelated to matrix degradation induced by proteases. An in vitro experiment showed that leucocyte elastase induces apoptosis in lung epithelial cells by changing mitochondrial permeability, mediated by a protease activated receptor 1 triggered pathway

Open Access
Scan to access more free content

To cite: Mimae T, Hagiyama M, Inoue T, *et al*. *Thorax* 2014;**69**:223–231.

involving activation of nuclear factor κB and p53.[5] Cathepsin S, a cysteine proteinase secreted from pulmonary macrophages, mediates alveolar epithelial cell apoptosis in interferon γ induced emphysema of mice by activating both mitochondrial and death receptor pathways.[6] Matrix metalloproteinases trigger activation of the death receptor apoptotic pathway by processing the tumour necrosis factor α precursor and Fas ligand to yield their bioactive forms.[7 8] These results suggest that excessive proteases can directly act on alveolar epithelial cells and cause apoptosis, but this possibility has not been intensively examined.

Cell adhesion molecule 1 (CADM1), also widely known as tumour suppressor in lung cancer 1 (TSLC1), is an intercellular adhesion molecule in the immunoglobulin superfamily. It is a membrane spanning glycoprotein composed of three extracellular immunoglobulin-like domains, a single transmembrane region and a short carboxy terminal intracytoplasmic tail with a protein 4.1 interaction sequence and a PDZ type II domain binding motif.[9] CADM1 localises to the lateral plasma membrane in pulmonary and biliary epithelia and binds *trans*-homophilically between adjacent cells.[10 11] Consequently, it is assumed to contribute to the integrity of epithelial cell structure and polarity.[12] Recent studies by our own and other laboratories have revealed that CADM1 expression is regulated by post-transcriptional mechanisms, including glycosylation and proteolytic cleavage, called shedding.[13 14] CADM1 is cleaved at two sites in its ectodomain, yielding two membrane associated C terminal fragments (CTF), termed αCTF and βCTF. This ectodomain shedding appears to occur on the plasma membrane because this event proceeds in isolated plasma membranes and is directly mediated by a membrane bound metalloprotease called a disintegrin and metalloproteinase 10 (ADAM10).[14] These CTFs are subsequently cleaved within the plasma membrane by γ secretase, yielding an intracellular domain (ICD).[14] Although we previously proposed CADM1 shedding as a candidate mechanism for downregulating full length CADM1,[14] it remains unknown whether the products generated by shedding (ie, CTFs and ICD) have any biological function.

In the present study, we compared CADM1 expression between emphysematous and normal lungs and found that αCTF and βCTF increased in emphysematous lungs in association with increased ectodomain shedding of CADM1. Because alveolar cell apoptosis also increased in emphysematous lungs, we then examined the possible association between CADM1 ectodomain shedding and alveolar cell apoptosis. Human lung epithelial cells were induced to express endogenous αCTF by shedding inducers and were transfected to express exogenous αCTF. Cell fractionation and immunofluorescence experiments revealed that αCTF localised to mitochondria. This localisation appeared to result in mitochondrial depolarisation and induction of cell apoptosis. These data identify CADM1-αCTF as a key molecule that links two landmark events in emphysema, proteolysis and apoptosis.

MATERIALS AND METHODS

All materials and methods used in this study are described in detail in the online supplementary methods.

RESULTS

Increased shedding of CADM1 in emphysematous lungs

Surgically resected lungs were examined histologically by pathologists (see online supplementary figure S1), and 10 normal subjects and 11 patients with emphysematous lungs were enrolled. Patient characteristics are summarised in table 1. The histological diagnosis was consistent with the results of preoperative respiratory function tests, except that three subjects with normal lungs (case Nos 5, 8 and 9) had low carbon monoxide transfer factor (Tlco) and one patient with emphysematous lungs (case No 13) had fairly good forced expiratory volume at 1 s (FEV_1)/forced vital capacity (FVC) and Tlco. All patients with emphysematous lungs were cigarette smokers, as revealed by their Brinkman Indices (table 1). Based on this observation and our previous finding that smoking may alter CADM1 expression in the lung,[15] we subgrouped subjects with normal lungs into smokers (n=5) and non-smokers (n=5). The lung tissue lysates were analysed by western blotting with a polyclonal antibody raised against the CADM1 C terminal 15 amino acid peptide. CADM1 αCTF, βCTF and ICD were recognisable by this antibody. The full length form of CADM1 and its two shed forms, αCTF and βCTF, were detected at about 100, 20 and 35 kDa, respectively (figure 1A). Bands detected at 50 and 25 kDa corresponded to the non-glycosylated full length form and βCTF, respectively, as we reported previously.[11] The expression level of the full length form normalised to β-actin decreased significantly in emphysematous lungs compared with normal lungs (figure 1B). This might be attributable to a low content of epithelial cells in the tissue lysates because emphysematous lungs have a lower number of alveolar epithelial cells, the major source of CADM1 in the peripheral lung.[10] This speculation was supported by a western blot reprobed with an antibody against E-cadherin, an epithelial cell marker,[10] which revealed that the full length form of CADM1 and E-cadherin levels were well correlated in normal (R^2=0.734; p<0.001) and emphysematous (R^2=0.586; p<0.001) lungs (see online supplementary figure S2).

Table 1 Clinical characteristics of patients with normal and emphysematous lungs

	Normal (non-smoker)					Normal (smoker)					Emphysema (smoker)										
Case	1	2	3	4	5	6	7	8	9	10	11	12	13	14	15	16	17	18	19	20	21
Age (years)	64	50	48	63	76	60	56	80	71	84	79	62	62	68	76	58	80	70	70	84	79
Sex	F	M	M	F	F	M	F	M	M	M	M	M	M	M	M	F	F	M	M	M	M
Brinkman Index	0	0	0	0	0	900	500	2400	1000	2220	980	800	1600	1600	1000	600	200	1000	1000	1280	1200
Cause of surgery	AD	AD	AD	AD	AD	AD	AD	SCLC	SQ	AD	SQ	AD	AD	PC	AD	AD	AD	SCLC	CH	SQ	AD
Excised lung lobe*	RL	RU	RU	RU	LL	RU	RL	RU	RL	LU	RU	RU	RU	LU	LU	RU	RL	RU	RM	RU	RL
FEV_1/FVC	82.3	80.5	86.6	86.8	79.9	73.0	76.7	76.6	78.1	84.1	61.7	73.2	75.1	55.0	88.8	58.1	74.6	76.7	73.0	83.5	61.5
Tlco (%)	101.8	NE	92.8	76.5	49.3	102.0	81.2	57.0	41.2	89.3	37.8	NE	71.2	NE	44.4	36.8	55.3	54.8	53.0	36.3	68.2

AD, adenocarcinoma; CH, chondroid hamartoma; FEV_1, forced expiratory volume in 1 s; FVC, forced vital capacity; NE, not examined; PC, plemorphic carcinoma; SCLC, small cell lung carcinoma; SQ, squamous cell carcinoma; Tlco, carbon monoxide transfer factor.
*LL, left lower; LU, left upper; RL, right lower; RM, right middle; RU, right upper.

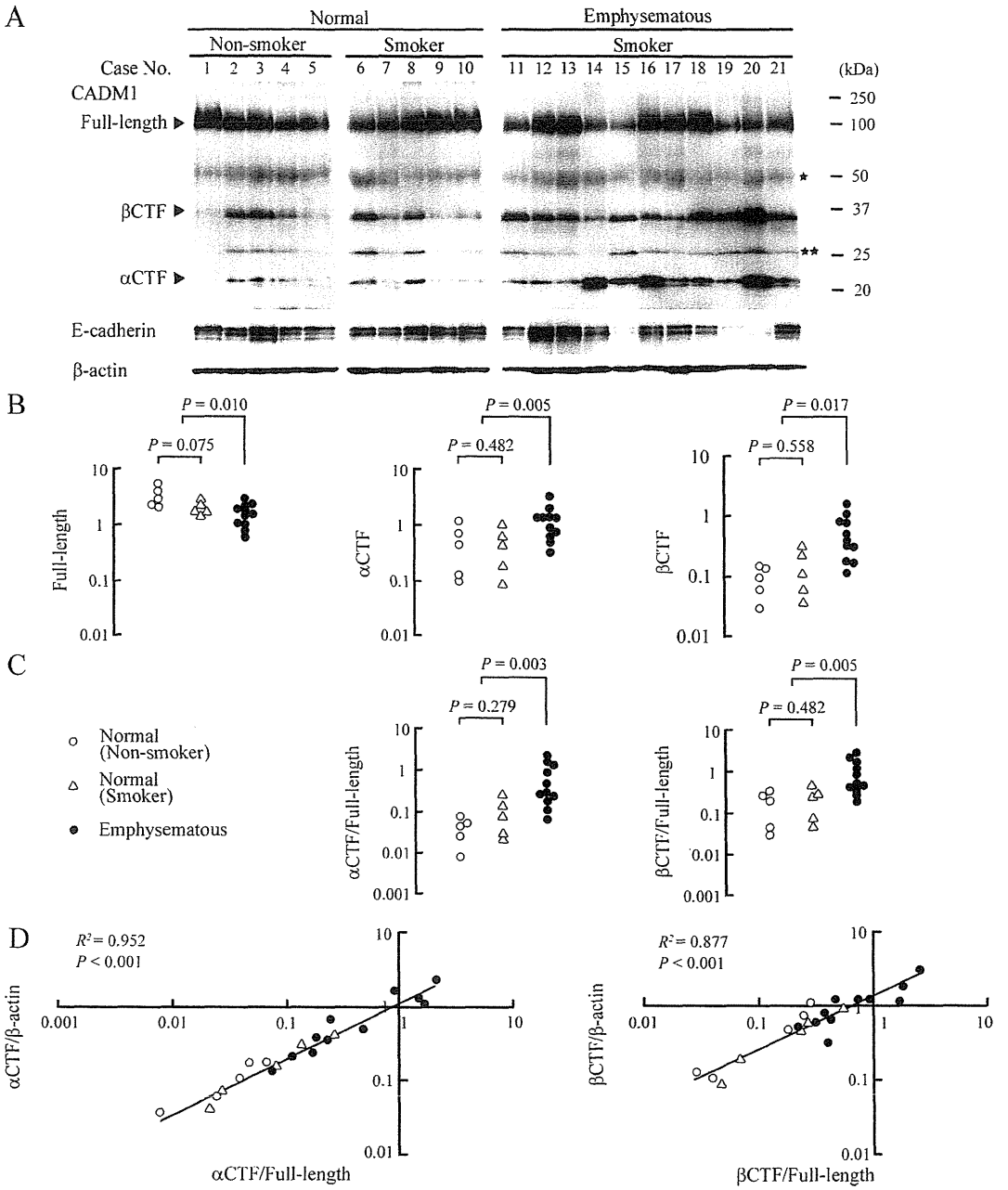

Figure 1 Increased ectodomain shedding of cell adhesion molecule 1 (CADM1) in emphysematous lungs. (A) Western blot analyses of CADM1 and E-cadherin in normal and emphysematous lungs. Cases are numbered as in table 1. Bands corresponding to the non-glycosylated full length form and β C terminal fragment (CTF) are depicted by one and two asterisks, respectively. The blots were reprobed with an anti-β-actin antibody to indicate protein loading per lane. (B) Graphs plotted with dots indicating relative expression levels of CADM1 molecules. In each lane of (A), intensities of bands specific to CADM1 full length form, αCTF and βCTF, and β-actin were quantified using NIH ImageJ software, and the intensities of CADM1 molecules were normalised to β-actin. Statistical significance was analysed by the Mann–Whitney U test, and p values are shown. (C) Graphs plotted with dots indicating expression levels of αCTF and βCTF relative to the full length form of CADM1. Statistical significance was analysed by the Mann–Whitney U test, and p values are shown. (D) Graphs with X and Y axes in band intensity ratios. On the left, αCTF/full length and αCTF/β-actin were plotted on the X and Y axes, respectively. On the right, βCTF/full length and βCTF/β-actin were plotted on the X and Y axes, respectively. In each graph, the two ratios were well approximated as linear. Correlations and statistical significance were analysed by Spearman's rank test, and R^2 and p values are shown.

In contrast, expression levels of αCTF and βCTF increased significantly in emphysematous lungs, while they were comparable between smokers and non-smokers with normal lungs (figure 1B). We also calculated the signal intensity ratios of αCTF and βCTF to the full length form for each case, and found that these ratios were significantly higher in emphysematous lungs than those in normal lungs (figure 1C), and were strongly positively correlated with αCTF and βCTF levels (R^2=0.952 and 0.877; p<0.001), respectively (figure 1D). The ratios of the two shed forms were comparable between smokers and non-smokers with normal lungs. These results indicate that CADM1 ectodomain shedding was

accelerated to generate more αCTF and βCTF in emphysematous lungs.

Increased apoptosis of alveolar cells in emphysematous lungs

Lung sections were double stained by the terminal deoxynucleotidyl transferase mediated dUTP nick end labelling (TUNEL; green) and E-cadherin immunofluorescence (red) (figure 2A, B). Alveolar epithelial cells were identified by membranous staining for E-cadherin. Practically all alveolar cells were TUNEL negative in normal lungs, irrespective of smoking habit, whereas >10% of alveolar cells on average were TUNEL positive in emphysematous lungs ($p<0.002$) (figure 2C).

CADM1-αCTF localises to mitochondria

To probe for a possible link between increased CADM1 ectodomain shedding and increased alveolar cell apoptosis, we used NCI-H441 cells, a human lung epithelial cell line with characteristics of Clara cells. Western blot analyses detected abundant expression of the full length form of CADM1 in NCI-H441 cells grown under standard culture conditions, but the two shed forms αCTF and βCTF were undetectable, indicating that CADM1 was rarely shed in steady state NCI-H441 cells. We used phorbol 12-myristate 13-acetate (PMA) and trypsin to induce CADM1 shedding, which both induce ectodomain shedding of transmembrane proteins.[14 16] When the cells were treated with a mixture of PMA (200 nM) and trypsin (0.0125% w/v, a concentration low enough to prevent cell detachment) for 20 min, but not with either alone, a considerable amount of αCTF appeared with a slight decrease in the amount of full length CADM1, indicating that CADM1 ectodomain shedding was induced by the treatment (figure 3). The reason why βCTF was not produced by the treatment is unknown. Considering that β shedding of β-amyloid precursor protein, a key event in Alzheimer's disease, occurs within cells,[17] trypsin may have no potential to activate β shedding due to its inaccessibility to β-sheddase(s).

PMA and trypsin treated or untreated cells were then double stained by CADM1 immunofluorescence and Mitotracker dye, a mitochondrial marker. CADM1 immunostaining was exclusively

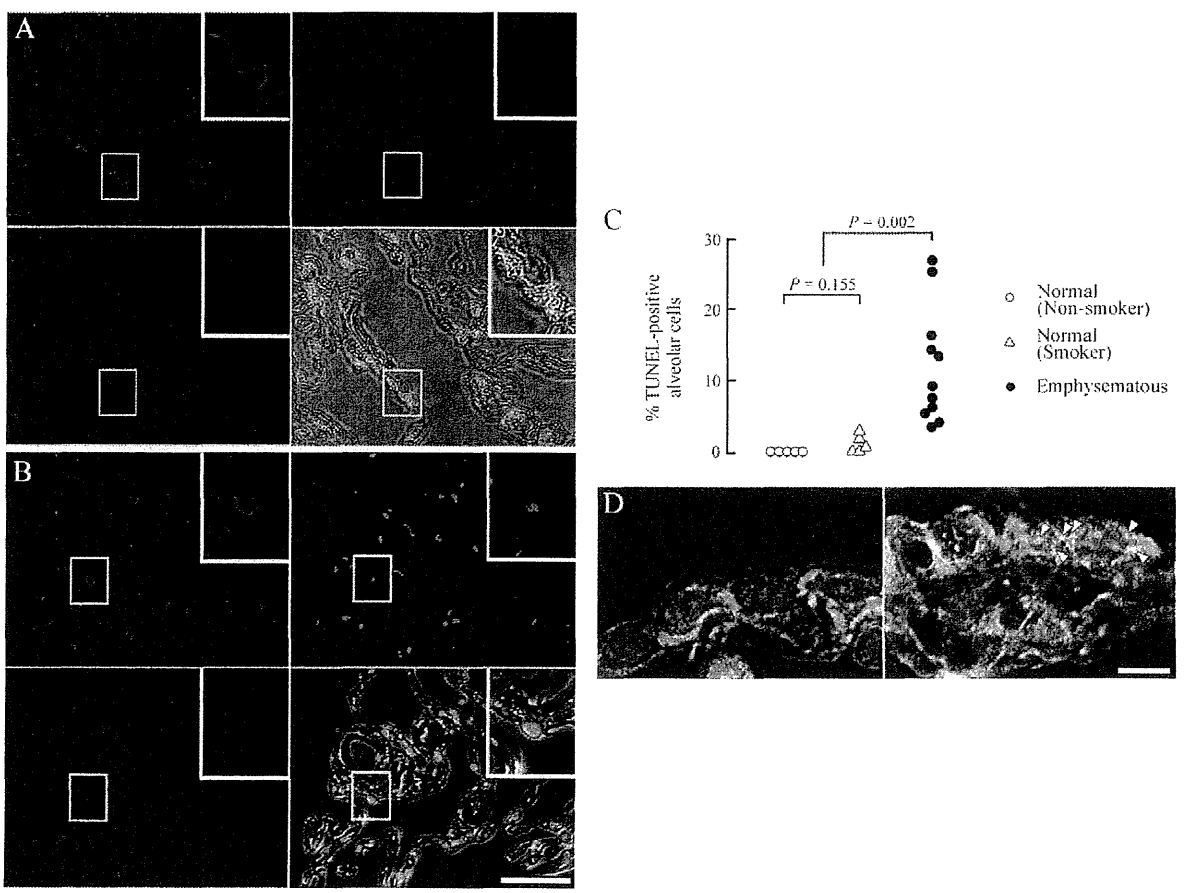

Figure 2 Increased apoptosis of alveolar epithelial cells in emphysematous lungs. (A, B) Representative results of terminal deoxynucleotidyl transferase dUTP nick end labelling (TUNEL) assays for normal (A) and emphysematous (B) lungs. Formalin fixed, paraffin embedded lung sections were triple stained by E-cadherin immunofluorescence (red; left upper), the TUNEL method (green; right upper) and 4′,6-diamino-2-phenylindole (DAPI, for nuclear counterstain; blue; left lower). These three images were merged on the differential interference contrast image (right lower). TUNEL negative and positive alveolar epithelial cells are enlarged in insets of (A) and (B), respectively. Bar=50 μm. (C) Graph plotted with dots indicating TUNEL positive alveolar epithelial cell proportions in individual patients who were divided into two groups, normal and emphysematous lungs. The normal lung patients were further divided into non-smokers and smokers. Statistical significance was analysed between groups by the Student's t test, and p values are shown. (D) Double immunofluorescence of normal (left) and emphysematous (right) lung sections for cell adhesion molecule 1 (CADM1) (green) and mitochondria (clone 113–1; red). Sections were counterstained by DAPI (blue). Three fluorescence images are merged on the differential interference contrast image. Arrowheads point to examples of colocalisation of CADM1 and mitochondrial immunostaining. Bar=10 μm.

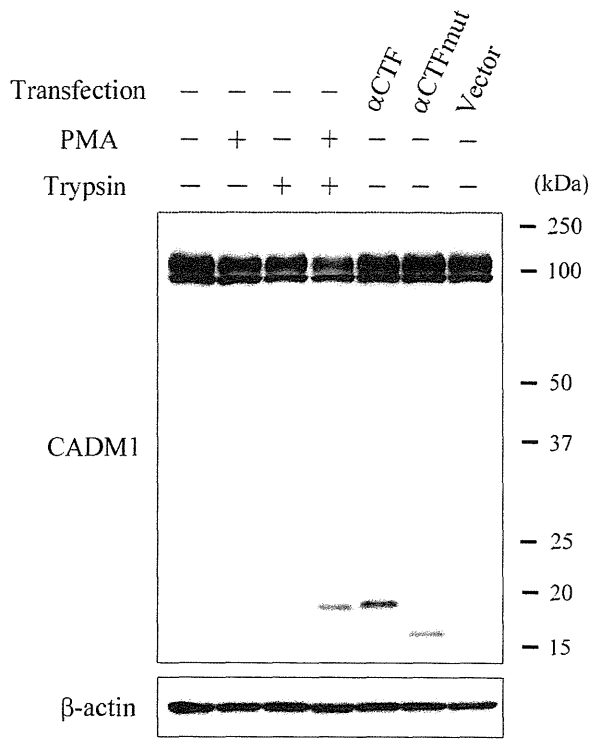

Figure 3 Induction of cell adhesion molecule 1 (CADM1) ectodomain shedding and exogenous expression of α C terminal fragment (CTF) and αCTFmut in NCI-H441 cells. NCI-H441 cells were treated with either phorbol myristic acid (PMA 200 nM) or trypsin (0.0125% w/v), or a mixture of both, or were transfected with pCX4bsr-SP-αCTF, pCX4bsr-SP-αCTFmut or an empty vector. After 20 min of treatment and 2 days of transfection, the cells were subjected to western blot analyses with the CADM1 antibody.

detected on the cell membrane of untreated cells (figure 4Aa), whereas PMA and trypsin treatment resulted in a marked appearance of cytoplasmic stains for CADM1, which were significantly colocalised with Mitotracker stain (figure 4Ab, B), suggesting subcellular localisation of CADM1-αCTF to mitochondria.

We examined this possibility by expressing αCTF exogenously. Because CADM1 ectodomain shedding likely occurs on the cell surface,[14] αCTF should be primarily a transmembrane protein. Thus according to our previous mass spectrometric data that determined the N terminal amino acid residue of αCTF,[14] we constructed a plasmid vector expressing a large deletion form of CADM1, in which the signal peptide was ligated upstream of αCTF (pCX4bsr-SP-αCTF). We mutated the intracytoplasmic domain of αCTF as a control so that the resulting domain would not target to mitochondria but to the cytosol (pCX4bsr-SP-αCTFmut; online supplementary figure S3), according to an intracellular localisation prediction algorithm (WoLF PSORT; refer to online supplementary methods). We transfected NCI-H441 cells with either plasmid construct, and 2 days later confirmed that the transfectants expressed a considerable amount of exogenous αCTF or αCTFmut by western blot analyses (figure 3). The ratios of αCTF to full length CADM1 in transfectants were equivalent to those in emphysematous lungs (see online supplementary figure S4). Taken together with the western blot results indicating that endogenous full length CADM1 in NCI-H441 cells was certainly lower than that in normal lung epithelial cells in vivo (see online supplementary figure S4), transfectants with pCX4bsr-SP-αCTF were considered to resemble epithelial cells from emphysematous lungs rather than normal lungs, in terms of CADM1 protein levels.

NCI-H441 transfectants were double stained with CADM1 immunofluorescence and Mitotracker dye. Transfectants with pCX4bsr-SP-αCTF exhibited a staining pattern quite similar to that of PMA and trypsin treated cells; the cytoplasmic CADM1 signals were well colocalised with Mitotracker stain (figure 4Ac, B). In contrast, pCX4bsr-SP-αCTFmut transfectants showed a strong CADM1 membranous staining with weak but significant cytoplasmic signals that were rarely colocalised with Mitotracker stain (figure 4Ad, B).

Mitochondrial localisation of αCTF was examined by cell fractionation of NCI-H441 cells expressing endogenous and exogenous αCTF. Exogenous αCTF and αCTFmut were expressed as N terminally FLAG tagged forms to clearly distinguish them from endogenous αCTF using the p3xFLAG-CMV-9 vector, which is designed to deliver the protein encoded by the cDNA insert efficiently to the cell surface. Expression of FLAG tagged proteins was confirmed by western blotting with an anti-FLAG antibody (see online supplementary figure S5). Transfected or untransfected NCI-H441 cells were treated with a mixture of PMA (200 nM) and trypsin (0.25% w/v) for 20 min to induce endogenous αCTF and detach cells without mitochondrial damage and then were fractionated into cytosolic and mitochondrial fractions. Whole cytoplasmic lysates without nuclei were also prepared from aliquots of the treated cells. Successful fractionation was verified by western blotting analyses, showing enrichment of glyceraldehyde 3-phosphate dehydrogenase (G3PDH), a cytosolic marker, and cytochrome c oxidase subunit IV (CoxIV), a mitochondrial marker, in the corresponding fractions (figure 5). Reprobing with the CADM1 antibody revealed that both endogenous and exogenous αCTFs were detected exclusively in the mitochondrial fraction as CoxIV, whereas αCTFmut was enriched in the cytosolic fraction as greatly as G3PDH (figure 5).

Lung sections were double stained with antibodies against CADM1 and mitochondria. CADM1 immunostaining in alveolar epithelial cells was primarily membranous in normal lungs whereas it was occasionally both membranous and cytoplasmic in emphysematous lungs and cytoplasmic staining was appreciably colocalised with mitochondrial staining (figure 2D). The proportion of epithelial cells with this colocalisation signal was significantly larger in emphysematous lungs (n=4) than in normal lungs (n=4) (11.3±8.3 vs 1.8±1.5%; p=0.038).

CADM1-αCTF decreases mitochondrial membrane potential and induces apoptosis

We examined whether CADM1-αCTF might alter mitochondrial membrane potential ($\Delta\Psi m$) that normally exists across the inner mitochondrial membrane using the JC-1 probe, a lipophilic cationic dye that exhibits $\Delta\Psi m$ dependent accumulation in mitochondria, as indicated by a fluorescence shift from green (~525 nm) to red (~590 nm). NCI-H441 transfectants expressing exogenous αCTF or αCTFmut were stained with JC-1 dye at 24, 48 and 72 h post-transfection, and mitochondrial depolarisation was assessed by measuring the red/green fluorescence intensity ratio of the dye (figure 6A and see online supplementary figure S6). αCTFmut did not change the JC-1 ratio at any time point, whereas αCTF significantly decreased the ratio at 48 and 72 h (figure 6B). Transfected and untransfected NCI-H441 cells were stained by the TUNEL technique 48 h after transfection. αCTFmut did not change the proportion

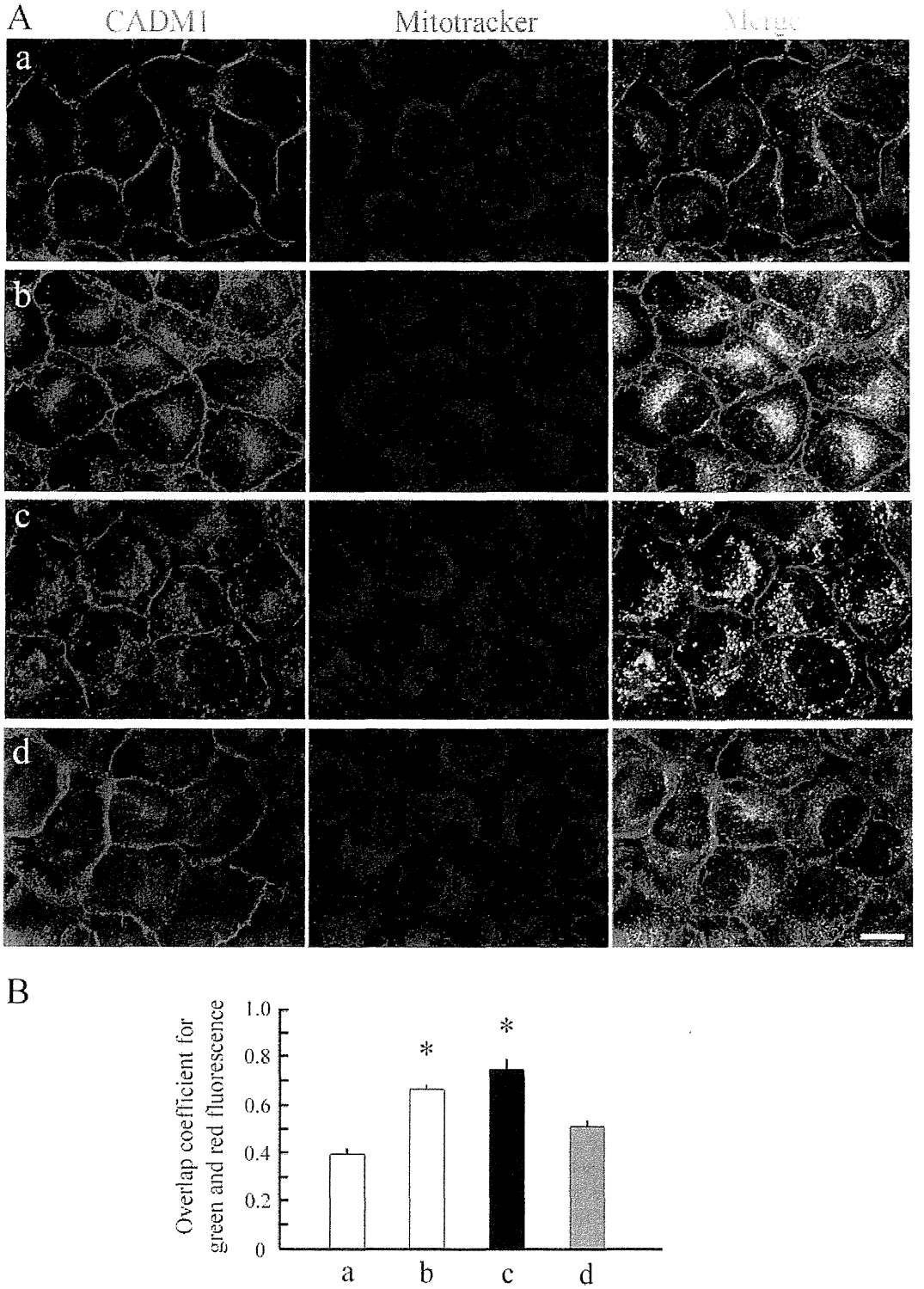

Figure 4 Immunofluorescence of cell adhesion molecule 1 (CADM1) with Mitotracker staining in NCI-H441 cells expressing α C terminal fragment (CTF) and αCTFmut. (A) NCI-H441 cells were untreated (a) or treated with a mixture of phorbol myristic acid and trypsin (b), or were transfected with pCX4bsr-SP-αCTF (c) or pCX4bsr-SP-αCTFmut (d). Then, cells were double stained with CADM1 immunofluorescence (green; left) and Mitotracker fluorescence (red; middle). In the merged images (right), yellow areas mean colocalisation of both fluorescent signals—that is, mitochondrial localisation of CADM1. Bar=10 μm. (B) Graph showing overlap coefficients in NCI-H441 cells of the four types (a–d shown in (A)). Intensity correlation between green and red fluorescence was quantified using ImageJ Colocalisation Analysis, and overlap coefficients were calculated. Data are expressed as mean±SD, and statistical significance was analysed by the Student's t test. *p<0.01 compared with the value of untreated cells (a in (A)).

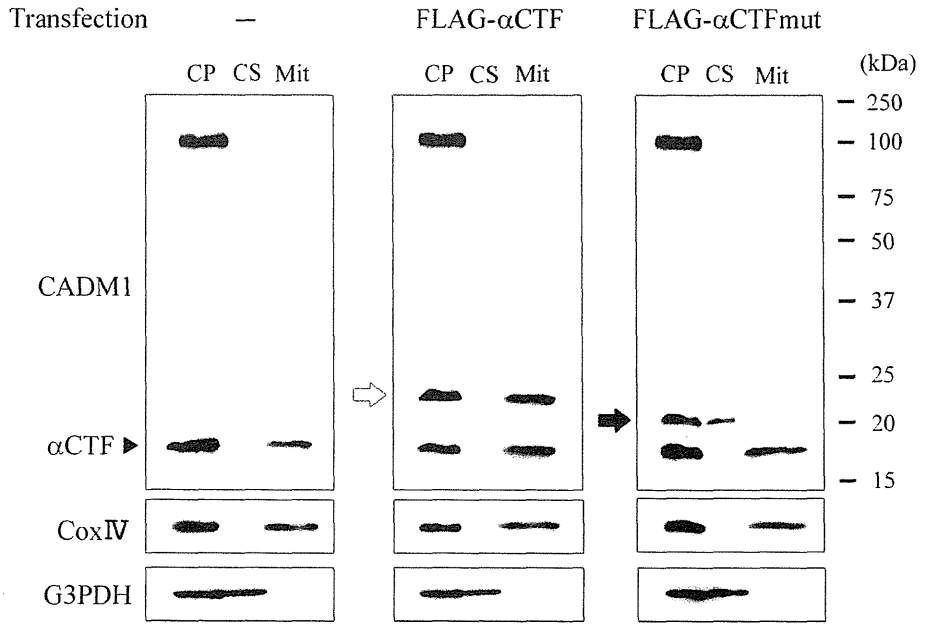

Figure 5 Cell fractionation experiments of NCI-H441 cells expressing α C terminal fragment (CTF) and αCTFmut. NCI-H441 cells were untransfected (left) or transfected with p3xFLAG-αCTF (middle) or p3xFLAG-αCTFmut (right), and were fractionated into cytosolic (CS) and mitochondrial (Mit) fractions. Whole cytoplasmic lysates (CP) were extracted from aliquots of the cells. These lysates and fractions were analysed with western blotting using antibodies against cell adhesion molecule 1 (CADM1), cytochrome c oxidase subunit IV (CoxIV) and glyceraldehyde 3-phosphate dehydrogenase (G3PDH). Open and closed arrows indicate FLAG tagged αCTF and αCTFmut, respectively.

of TUNEL positive cells whereas αCTF increased the proportion fivefold ($p<0.01$) (figure 6B).

DISCUSSION

We found that CADM1 ectodomain shedding increased in emphysematous lungs from smoking patients, but not in normal lungs from smoking patients, suggesting that oxidants in cigarette smoke may act as a critical inducer of CADM1 ectodomain shedding only in subjects who have particular genetic backgrounds. Of interest, changes in emphysema susceptible genes, such as α-1 antitrypsin,[18] macrophage elastase,[19] klotho[20] and surfactant D,[21] lead to a relative excess of proteases, creating a local protease/antiprotease imbalance.[19 21–23] In the present study, all patients with smoking habits were obliged to quit smoking more than 1 month before the date of surgery. Therefore, oxidants seem not to promote CADM1 shedding through its direct ongoing action but rather seem to help establish long lasting protease/antiprotease imbalances in alveoli.

All but one patient (case No 19) analysed in this study had lung cancer. Because CADM1 is known to be downregulated in lung cancer due to promoter methylation,[24] these patients had potentially impaired CADM1 expression even in non-cancerous lungs. We performed western blot analyses of a small number of emphysematous lungs that did not develop lung cancer, and detected a relative increase in αCTF and βCTF to full length CADM1 (see online supplementary figure S7). Increased amounts of αCTF and βCTF appeared to be present in emphysematous lungs as a result of increased ectodomain shedding of CADM1 in emphysematous lungs, both with and without lung cancer.

Cell fractionation and immunofluorescence experiments consistently showed that αCTF localised to mitochondria. This finding appeared to be relevant in vivo, as we detected intracytoplasmic CADM1 that was associated with mitochondria in alveolar epithelial cells from emphysematous lungs (figure 2D). Mutagenesis experiments revealed a decisive role for the intracytoplasmic domain in this subcellular localisation. How the intracytoplasmic domain leads αCTF to mitochondria remains to be addressed. A growing body of evidence is accumulating to show that cell membrane spanning proteins, such as epidermal growth factor receptor and mucin 1, can translocate to mitochondria.[25 26] Although mechanisms underlying these events remain largely unknown, clathrin mediated endocytosis is shown to be involved.[26] After internalisation, mucin 1 is assumed to utilise heat shock proteins as molecular chaperons for mitochondrial translocation.[25] Higashiyama *et al* demonstrated that the remnant peptides generated by ectodomain shedding of type I integral membrane proteins, such as pro-heparin binding epidermal growth factor-like growth factor and pro-amphiregulin, are internalised into endocytotic vesicles.[27 28] The N and C termini of the peptides are positioned inside and outside of the vesicles, respectively, and the C terminal tail, free in the cytosol, plays a decisive role in the intracellular destinations of the remnant peptide.[27 28] αCTF may be present as a vesicle associated transmembrane molecule in the cytoplasm, with its C terminal tail being free outside the vesicle, and this C terminal tail may carry a conformational signal that serves as a binding site for molecular chaperons, such as heat shock protein family members.

Exogenous αCTF decreased mitochondrial membrane potential in NCI-H441 cells and increased apoptosis, suggesting that mitochondrial localisation of αCTF might result in activation of the mitochondrial apoptosis pathway. Mao *et al* reported that exogenous CADM1 induces caspase 3 activation and apoptosis in A549 lung adenocarcinoma cells lacking endogenous CADM1, and that protein 4.1 binding motif and PDZ domain binding motif in the intracytoplasmic domain are indispensable for this induction.[29] Members of the membrane associated guanylate kinase (MAGuK) family are known as binding partners to the latter motif.[30] Interestingly, this family contains a subgroup that carries the caspase recruitment domain in its N terminal

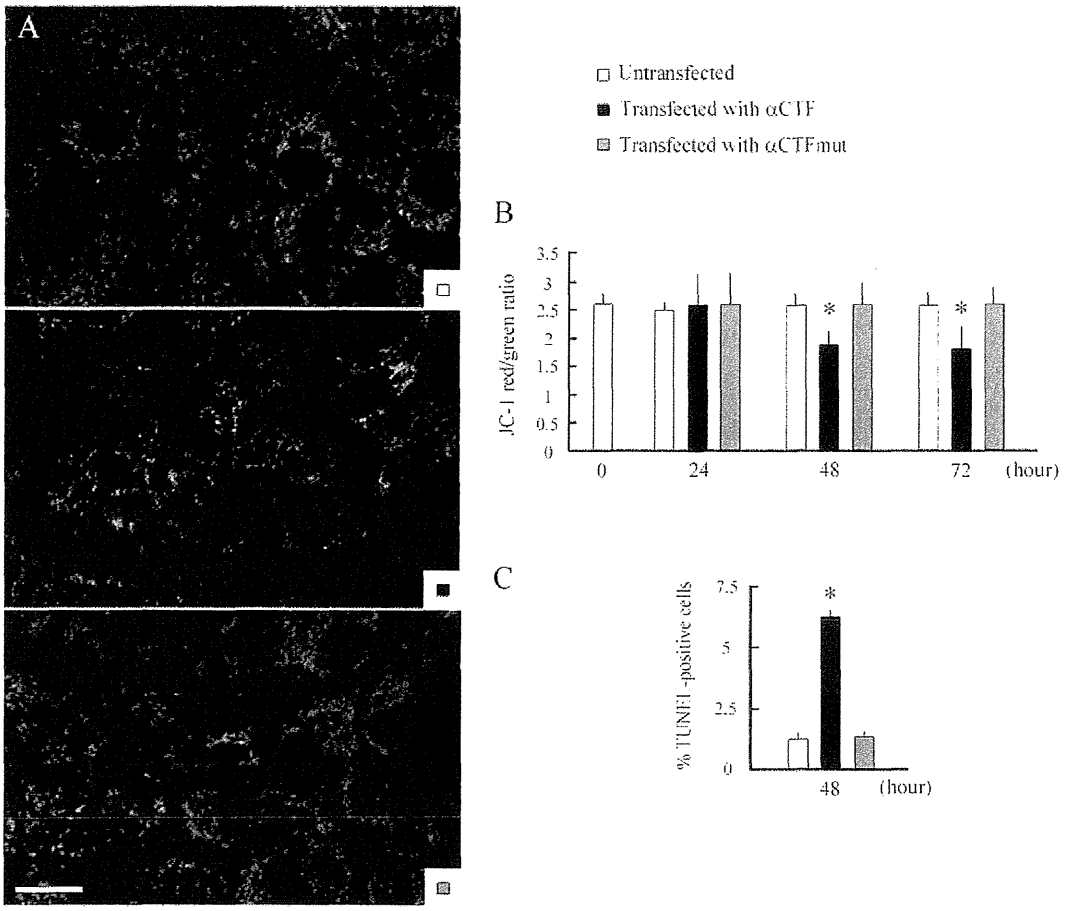

Figure 6 α C terminal fragment (CTF) decreases mitochondrial membrane potential in NCI-H441 cells and increases apoptosis. (A) Representative results of JC-1 staining in NCI-H441 cells. NCI-H441 cells were untransfected (upper) or transfected with pCX4bsr-SP-αCTF (middle) or pCX4bsr-SP-αCTFmut (lower), and were stained 48 h later with JC-1 dye. Images were captured by a confocal laser microscope, and green and red fluorescence signals were merged. Differential interference contrast images are shown in online supplementary figure S6. Bar=20 μm. (B) Graph showing changes in JC-1 red/green ratios in NCI-H441 cells after transfection. NCI-H441 cells were untransfected or transfected with pCX4bsr-SP-αCTF or pCX4bsr-SP-αCTFmut, and were stained with JC-1 dye at the indicated time points. Cells were observed through a confocal laser microscope and were morphometrically analysed to calculate JC-1 red/green ratios. Data are expressed as mean± SD, and statistical significance was analysed by the Student's t test. *p<0.01 compared with the value of untransfected cells. (C) Graph showing the proportion of terminal deoxynucleotidyl transferase dUTP nick end labelling (TUNEL) positive NCI-H441 cells at 2 days after transfection. Cells were transfected as in (B). After 2 days, cells were stained with the TUNEL method, and the proportions of TUNEL positive cells were calculated. Data are expressed as mean±SD, and statistical significance was analysed by the Mann–Whitney U test. *p<0.01 compared with the value in untransfected cells.

region and participates in apoptosis signalling.[31] αCTF and βCTF, which both share the intracytoplasmic domain, once produced, may activate the mitochondrial apoptosis pathway by transporting particular MAGuK family members to mitochondria in alveolar epithelial cells.

There are several splice variants of human CADM1, named isoforms SP1 to SP4.[32] Reverse transcription-PCR revealed that nine lungs examined and NCI-H441 cells all expressed SP4 exclusively (see online supplementary figure S8). Tanabe *et al* showed that SP1 and SP2 are shed constitutively, while SP3 is non-cleavable.[33] Our data proved SP4 cleavable. SP4 ectodomain shedding appeared to be not constitutive but induced by particular pathological stimuli. Moiseeva *et al* reported that SP4 overexpressing HMC-1 mast cells show better survival and lower caspase 3/7 activity than SP1 overexpressing cells.[34] This difference between two isoforms may be explained by their distinct susceptibility to ectodomain shedding. In HMC-1 cells, SP1 may produce more αCTF and/or βCTF than SP4, resulting in activation of the mitochondrial apoptosis pathway.

In conclusion, we propose increased ectodomain shedding of CADM1 as a novel molecular mechanism for increased alveolar cell apoptosis in emphysematous lungs. This mechanism is an extension of the conventional understanding that proteolytic activity is locally excessive in emphysematous lung alveoli because CADM1 ectodomain shedding per se is a proteolytic process, and also suggests that selective inhibitors to block CADM1 sheddase activity and/or mitochondrial localisation of CADM1 shedding products can slow or halt the progression of emphysema. In fact, ADAM10 is released by human alveolar macrophages, and intratracheal administration of an adenoviral vector expressing ADAM10 in mice results in the development of emphysema.[35] Further characterisation of CADM1 ectodomain shedding and its associated molecular events will open a new avenue for target based therapeutic approaches to emphysema.

Contributors AI and YM designed the study, and AI wrote the manuscript. AI, TM and MO provided the clinical samples. TM, MH, TI, AY and TK performed the experiments, and MH analysed the data.

Funding This study was supported by the Japan Society for the Promotion of Science Kakenhi (24890274 and 25860302 to MH, 24659184 to TI, 24890137 to TM, and 24590492 to AI), and grants from the Yasuda Medical Foundation and the Osaka Medical Research Foundation for Intractable Diseases.

Competing interests None.

Patient consent Obtained.

Ethics approval Ethics approval was provided by the ethics committee of Hiroshima University and Kinki University, Japan (approval Nos Eki-350 and 25–088).

Provenance and peer review Not commissioned; externally peer reviewed.

REFERENCES

1 Snider GL, Kleinerman J, Thurlbeck WM, *et al*. The definition of emphysema. Report of a National Heart, Lung, and Blood Institute, Division of Lung Diseases workshop. *Am Rev Respir Dis* 1985;132:182–85.
2 Tuder RM, Petrache I, Elias JA, *et al*. Apoptosis and emphysema: the missing link. *Am J Respir Cell Mol Biol* 2003;28:551–4.
3 Taraseviciene-Stewart L, Voelkel NF. Molecular pathogenesis of emphysema. *J Clin Invest* 2008;118:394–402.
4 Demedts IK, Demoor T, Bracke KR, *et al*. Role of apoptosis in the pathogenesis of COPD and pulmonary emphysema. *Respir Res* 2006;7:53.
5 Suzuki T, Yamashita C, Zemans RL, *et al*. Leukocyte elastase induces lung epithelial apoptosis via a PAR-1-, NF-kappaB-, and p53-dependent pathway. *Am J Respir Cell Mol Biol* 2009;41:742–55.
6 Zheng T, Kang MJ, Crothers K, *et al*. Role of cathepsin S-dependent epithelial cell apoptosis in IFN-gamma-induced alveolar remodeling and pulmonary emphysema. *J Immunol* 2005;174:8106–15.
7 Powell WC, Fingleton B, Wilson CL, *et al*. The metalloproteinase matrilysin proteolytically generates active soluble Fas ligand and potentiates epithelial cell apoptosis. *Curr Biol* 1999;9:1441–7.
8 Mohan MJ, Seaton T, Mitchell J, *et al*. The tumor necrosis factor-alpha converting enzyme (TACE): a unique metalloproteinase with highly defined substrate selectivity. *Biochemistry* 2002;41:9462–9.
9 Kuramochi M, Fukuhara H, Nobukuni T, *et al*. TSLC1 is a tumor-suppressor gene in human non-small-cell lung cancer. *Nat Genet* 2001;27:427–30.
10 Ito A, Okada M, Uchino K, *et al*. Expression of the TSLC1 adhesion molecule in pulmonary epithelium and its down-regulation in pulmonary adenocarcinoma other than bronchioloalveolar carcinoma. *Lab Invest* 2003;83:1175–83.
11 Ito A, Nishikawa Y, Ohnuma K, *et al*. SgIGSF is a novel biliary-epithelial cell adhesion molecule mediating duct/ductule development. *Hepatology* 2007;45:684–94.
12 Sakurai-Yageta M, Masuda M, Tsuboi Y, *et al*. Tumor suppressor CADM1 is involved in epithelial cell structure. *Biochem Biophys Res Commun* 2009;390:977–82.
13 Fogel AI, Li Y, Giza J, *et al*. N-glycosylation at the SynCAM (synaptic cell adhesion molecule) immunoglobulin interface modulates synaptic adhesion. *J Biol Chem* 2010;285:34864–74.
14 Nagara Y, Hagiyama M, Hatano N, *et al*. Tumor suppressor cell adhesion molecule 1 (CADM1) is cleaved by a disintegrin and metalloprotease 10 (ADAM10) and subsequently cleaved by gamma-secretase complex. *Biochem Biophys Res Commun* 2012;417:462–7.
15 Kikuchi S, Yamada D, Fukami T, *et al*. Hypermethylation of the TSLC1/IGSF4 promoter is associated with tobacco smoking and a poor prognosis in primary nonsmall cell lung carcinoma. *Cancer* 2006;106:1751–8.
16 Ding K, Lopez-Burks M, Sanchez-Duran JA, *et al*. Growth factor-induced shedding of syndecan-1 confers glypican-1 dependence on mitogenic responses of cancer cells. *J Cell Biol* 2005;171:729–38.
17 Chyung AS, Greenberg BD, Cook DG, *et al*. Novel beta-secretase cleavage of beta-amyloid precursor protein in the endoplasmic reticulum/intermediate compartment of NT2N cells. *J Cell Biol* 1997;138:671–80.
18 Martorana PA, Brand T, Gardi C, *et al*. The pallid mouse. A model of genetic alpha 1-antitrypsin deficiency. *Lab Invest* 1993;68:233–41.
19 Hautamaki RD, Kobayashi DK, Senior RM, *et al*. Requirement for macrophage elastase for cigarette smoke-induced emphysema in mice. *Science* 1997;277:2002–4.
20 Kuro-o M, Matsumura Y, Aizawa H, *et al*. Mutation of the mouse klotho gene leads to a syndrome resembling ageing. *Nature* 1997;390:45–51.
21 Wert SE, Yoshida M, LeVine AM, *et al*. Increased metalloproteinase activity, oxidant production, and emphysema in surfactant protein D gene-inactivated mice. *Proc Natl Acad Sci U S A* 2000;97:5972–7.
22 Kidokoro Y, Kravis TC, Moser KM, *et al*. Relationship of leukocyte elastase concentration to severity of emphysema in homozygous alpha1-antitrypsin-deficient persons. *Am Rev Respir Dis* 1977;115:793–803.
23 Funada Y, Nishimura Y, Yokoyama M. Imbalance of matrix metalloproteinase-9 and tissue inhibitor of matrix metalloproteinase-1 is associated with pulmonary emphysema in Klotho mice. *Kobe J Med Sci* 2004;50:59–67.
24 Fukami T, Fukuhara H, Kuramochi M, *et al*. Promoter methylation of the TSLC1 gene in advanced lung tumors and various cancer cell lines. *Int J Cancer* 2003;107:53–9.
25 Ren J, Bharti A, Raina D, *et al*. MUC1 oncoprotein is targeted to mitochondria by heregulin-induced activation of c-Src and the molecular chaperone HSP90. *Oncogene* 2006;25:20–31.
26 Demory ML, Boerner JL, Davidson R, *et al*. Epidermal growth factor receptor translocation to the mitochondria: regulation and effect. *J Biol Chem* 2009;284:36592–604.
27 Hieda M, Isokane M, Koizumi M, *et al*. Membrane-anchored growth factor, HB-EGF, on the cell surface targeted to the inner nuclear membrane. *J Cell Biol* 2008;180:763–9.
28 Isokane M, Hieda M, Hirakawa S, *et al*. Plasma-membrane-anchored growth factor pro-amphiregulin binds A-type lamin and regulates global transcription. *J Cell Sci* 2008;121:3608–18.
29 Mao X, Seidlitz E, Truant R, *et al*. Re-expression of TSLC1 in a non-small-cell lung cancer cell line induces apoptosis and inhibits tumor growth. *Oncogene* 2004;23:5632–42.
30 Murakami Y. Involvement of a cell adhesion molecule, TSLC1/IGSF4, in human oncogenesis. *Cancer Sci* 2005;96:543–52.
31 Bertin J, Wang L, Guo Y, *et al*. CARD11 and CARD14 are novel caspase recruitment domain (CARD)/membrane-associated guanylate kinase (MAGUK) family members that interact with BCL10 and activate NF-kappa B. *J Biol Chem* 2001;276:11877–82.
32 Biederer T. Bioinformatic characterization of the SynCAM family of immunoglobulin-like domain-containing adhesion molecules. *Genomics* 2006;87:139–50.
33 Tanabe Y, Kasahara T, Momoi T, *et al*. Neuronal RA175/SynCAM1 isoforms are processed by tumor necrosis factor-alpha-converting enzyme (TACE)/ADAM17-like proteases. *Neurosci Lett* 2008;444:16–21.
34 Moiseeva EP, Leyland ML, Bradding P. CADM1 is expressed as multiple alternatively spliced functional and dysfunctional isoforms in human mast cells. *Cell Mol Life Sci* 2012;69:2751–64.
35 Saitoh H, Leopold PL, Harvey BG, *et al*. Emphysema mediated by lung overexpression of ADAM10. *Clin Transl Sci* 2009;2:50–6.

CHEST Original Research
LUNG CANCER

Appropriate Sublobar Resection Choice for Ground Glass Opacity-Dominant Clinical Stage IA Lung Adenocarcinoma

Wedge Resection or Segmentectomy

Yasuhiro Tsutani, MD, PhD; Yoshihiro Miyata, MD, PhD; Haruhiko Nakayama, MD, PhD; Sakae Okumura, MD, PhD; Shuji Adachi, MD, PhD; Masahiro Yoshimura, MD, PhD; and Morihito Okada, MD, PhD

Background: **The purpose of this multicenter study was to characterize ground glass opacity (GGO)-dominant clinical stage IA lung adenocarcinomas and evaluate prognosis of these tumors after sublobar resection, such as segmentectomy and wedge resection.**
Methods: **We evaluated 610 consecutive patients with clinical stage IA lung adenocarcinoma who underwent complete resection after preoperative high-resolution CT scanning and ^{18}F-fluorodeoxyglucose PET/CT scanning and revealed 239 (39.2%) that had a >50% GGO component.**
Results: **GGO-dominant tumors rarely exhibited pathologic invasiveness, including lymphatic, vascular, or pleural invasion and lymph node metastasis. There was no significant difference in 3-year recurrence-free survival (RFS) among patients who underwent lobectomy (96.4%), segmentectomy (96.1%), and wedge resection (98.7%) of GGO-dominant tumors ($P = .44$). Furthermore, for GGO-dominant T1b tumors, 3-year RFS was similar in patients who underwent lobectomy (93.7%), segmentectomy (92.9%), and wedge resection (100%, $P = .66$). Two of 84 patients (2.4%) with GGO-dominant T1b tumors had lymph node metastasis. Multivariate Cox analysis showed that tumor size, maximum standardized uptake value on ^{18}F-fluorodeoxyglucose PET/CT scan, and surgical procedure did not affect RFS in GGO-dominant tumors.**
Conclusions: **GGO-dominant clinical stage IA lung adenocarcinomas are a uniform group of tumors that exhibit low-grade malignancy and have an extremely favorable prognosis. Patients with GGO-dominant clinical stage IA adenocarcinomas can be successfully treated with wedge resection of a T1a tumor and segmentectomy of a T1b tumor.** ***CHEST 2014; 145(1):66–71***

Abbreviations: FDG = ^{18}F-fluorodeoxyglucose; FOV = field of view; GGO = ground glass opacity; HRCT = high-resolution CT; HU = Hounsfield units; IRB = institutional review board; NSCLC = non-small cell lung cancer; OS = overall survival; RFS = recurrence-free survival; SUVmax = maximum standardized uptake value

Advances in radiologic techniques, such as high-resolution CT (HRCT) scanning and the widespread use of low-dose helical CT screening, have enabled frequent detection of early lung adenocarcinoma.[1-3] On HRCT scan, early lung adenocarcinoma often contains a nonsolid component, such as ground glass opacity (GGO), that is closely associated with a pathologic lepidic growth component.[4,5] Patients with GGO-dominant small lung adenocarcinoma are believed to have a good prognosis.[6] A recent study also demonstrated that patients with GGO-dominant clinical T1N0M0 lung adenocarcinoma (consolidation/tumor ratio ≤ 0.5 on thin-section CT scan) have an excellent prognosis after lobectomy.[7] Although patients with GGO-dominant tumors may be candidates for sublobar resection, there is no clear evidence to support this hypothesis.

For editorial comment see page 9

A prospective study that compared sublobar resection (wedge resection or segmentectomy) concomitant with lobectomy for clinical T1N0M0 non-small cell lung cancer (NSCLC) concluded that sublobar resection resulted in a high local recurrence and a low

survival rate.[8] However, sublobar resection for early lung cancer has been debated for a considerable amount of time. Several studies have demonstrated the usefulness of sublobar resection for peripheral small-sized NSCLC.[3,9-12] However, there currently is little evidence in patients who are optimal candidates for sublobar resection. Therefore, the present study aimed to characterize GGO-dominant clinical stage IA lung adenocarcinomas and to evaluate the prognosis of patients with these tumors after sublobar resection.

Materials and Methods

Patients

We evaluated the results of ^{18}F-fluorodeoxyglucose (FDG) PET/CT scans of 610 patients with clinical T1N0M0 stage IA lung adenocarcinoma from four institutions (Hiroshima University, Kanagawa Cancer Center, Cancer Institute Hospital, and Hyogo Cancer Center, Japan) between August 1, 2005, and June 30, 2010. Patients with incompletely resected tumors (R1 or R2) and those with multiple tumors or who had previously undergone lung surgeries were not included in our prospectively maintained database. Patient data obtained from this multicenter database were retrospectively analyzed for this study.

Patients underwent HRCT scanning and FDG-PET/CT scanning followed by curative R0 resection, and their tumors were staged according to the seventh edition of the *TNM Classification of Malignant Tumors*.[13] Mediastinoscopy or endobronchial ultrasonography was not routinely performed because all patients had undergone preoperative HRCT scanning and FDG-PET/CT scanning. HRCT scanning and FDG-PET/CT scanning revealed an absence of a >1 cm enlargement in mediastinal or hilar lymph nodes and an absence of >1.5 accumulation for the maximum standardized uptake value (SUVmax) in these lymph nodes, respectively. Sublobar resection was allowed in patients with complete disease removal as an optional procedure for a peripheral clinical T1N0M0 tumor that was intraoperatively assessed as N0 by frozen section evaluation of enlarged lymph nodes or by ensuring that there was no obvious enlargement of lymph nodes in the thoracic cavity. Systematic lymph node dissection, such as that of hilar and mediastinal nodes, was performed during segmentectomy but not during wedge resection. All patients showing pathologic lymph node metastasis received four cycles of platinum-based chemotherapy after surgery.

The inclusion criteria were preoperative staging determined through HRCT scan and FDG-PET/CT scan, curative surgery without neoadjuvant chemotherapy or radiotherapy, and a definitive histopathologic diagnosis of lung adenocarcinoma. This study was approved by the institutional review boards (IRBs) of the participating institutions (Hiroshima University Hospital IRB, No. EKI-644; Kanagawa Cancer Center IRB, No. KEN-31; Cancer Institute Hospital IRB, No. 2008-1018; Hyogo Cancer Center IRB, No. H20-RK-15). The requirement of informed consent from individual patients was waived because this study was a retrospective review of a patient database.

HRCT Scanning

Sixteen-row multidetector CT scanning was used to independently acquire chest images of subsequent FDG-PET/CT image examinations. The following parameters were used to acquire high-resolution tumor images: 120 kVp, 200 mA, 1- to 2-mm section thickness, 512×512-pixel resolution, 0.5- to 1.0-s scanning time, high-spatial reconstruction algorithm with a 20-cm field of view (FOV), and mediastinal (level, 40 Hounsfield units [HU]; width, 400 HU) and lung (level, -600 HU; width, 1,600 HU) window settings. GGO was defined as a misty increase in lung attenuation without obscuring the underlying vascular markings. A GGO-dominant tumor was defined as having a $>50\%$ GGO component. We defined a solid tumor size as the maximum dimension of the solid component measured on lung window settings, excluding GGO.[14] CT scans were reviewed and tumor sizes determined by radiologists from each institution.

FDG-PET/CT Scanning

Patients were instructed to fast for ≥ 4 h before IV injection of 74 to 370 MBq FDG and were subsequently advised to rest for ≥ 1 h before FDG-PET/CT scanning. Blood glucose levels were determined before tracer injection to confirm a <150 mg/dL level. Patients with blood glucose levels of ≥ 150 mg/dL were excluded from imaging. For imaging, a Discovery ST (GE Healthcare), an Aquiduo (Toshiba Medical Systems Corporation), or a Biograph Sensation 16 (Siemens AG) integrated three-dimensional PET/CT scanner was used. Low-dose, nonenhanced CT images of 2- to 4-mm section thickness for attenuation correction and localization of lesions identified with PET scan were acquired from head to pelvic floor in each patient by standard protocol.

Immediately after CT imaging, PET scanning was performed with an identical axial FOV for 2 to 4 min/table position, depending on condition of the patient and scanner performance. An iterative algorithm with CT scan-derived attenuation correction was used to reconstruct all PET images with a 50-cm FOV. We used an anthropomorphic body phantom (NEMA PET Sensitivity Phantom [NU2-2001]; Data Spectrum Corporation) to minimize variations in SUV among the institutions.[15] To decrease interinstitution SUV inconsistencies, a calibration factor was determined by dividing the actual SUV by the gauged mean SUV in the phantom background. The final SUV used in this study was referred to as the revised SUVmax.[16,17] The original SUVmax values were determined by radiologists from each institution.

Follow-up Evaluations

All patients who underwent lung resection were followed up from their day of surgery. For the first 2 years, postoperative follow-up procedures included a physical examination and chest roentgenogram every 3 months and chest and abdominal CT scan examinations every 6 months. Subsequently, a physical examination and chest roentgenogram were performed every 6 months, and a chest CT scan examination was performed each year.

Manuscript received May 6, 2013; revision accepted July 12, 2013.
Affiliations: From the Department of Surgical Oncology (Drs Tsutani, Miyata, and Okada), Hiroshima University, Hiroshima; Department of Thoracic Surgery (Dr Nakayama), Kanagawa Cancer Center, Yokohama; Department of Thoracic Surgery (Dr Okumura), Cancer Institute Hospital, Tokyo; and Department of Radiology (Dr Adachi) and Department of Thoracic Surgery (Dr Yoshimura), Hyogo Cancer Center, Akashi, Japan.
Funding/Support: The authors have reported to *CHEST* that no funding was received for this study.
Correspondence to: Morihito Okada, MD, PhD, Department of Surgical Oncology, Research Institute for Radiation Biology and Medicine, Hiroshima University, 1-2-3-Kasumi, Minami-ku, Hiroshima City, Hiroshima 734-0037, Japan; e-mail: morihito@hiroshima-u.ac.jp

DOI: 10.1378/chest.13-1094

Statistical Analysis

Results are presented as counts and percentages or as medians, unless stated otherwise. A χ^2 test was used to compare categorical variable frequencies. Fisher exact test was used when sample sizes were small. Recurrence-free survival (RFS) was defined as the time from the date of surgery until the first event (relapse or death from any cause) or the last follow-up. Overall survival (OS) was defined as the time from the date of surgery until death from any cause or the last follow-up. The Kaplan-Meier method was used to assess RFS and OS durations, and these were compared by log-rank test. To assess the potential independent effects of the surgical procedure on RFS, we used multivariate analyses with a Cox proportional hazards model. SPSS, version 10.5 (IBM Corporation) software was used for statistical analysis. The level of significance was set at $P < .05$.

Results

Table 1 shows the characteristics of patients with GGO-dominant tumors. Two hundred thirty-nine of 610 patients (39.2%) had GGO-dominant tumors that had a >50% GGO component. No 30-day postoperative mortality was observed for this population. The median follow-up period after surgery was 42.2 months. Patients with GGO-dominant tumors rarely had pathologically invasive tumors and lymph node metastases. Table 2 shows the distribution of operative procedures for each tumor size (clinical T1a and T1b). Sublobar resections, such as wedge resection and segmentectomy, were more likely performed in T1a tumors, whereas lobectomy was more likely performed in T1b tumors.

Recurrences developed in two patients with GGO-dominant tumors during the follow-up period (Table 3). One patient was an 82-year-old man with a 1.0-cm solid tumor size and with an SUVmax of 1.5 T1b (2.6 cm); peritoneal recurrence developed in this patient 23 months after left-sided S6 segmentectomy. The other patient was a 61-year-old woman with a 1.2-cm solid tumor size and a tumor SUVmax of 1.8 T1b (3.0 cm); brain metastasis developed in this patient 24 months after right-sided middle lobectomy.

Table 1—*Clinicopathologic Features of Patients With GGO-Dominant Tumors*

Variable	GGO-Dominant Tumors (n = 239)
Age, y	65 (31-89)
Male sex	94 (39.3)
Whole tumor size, cm	1.8 (0.7-3.0)
Solid tumor size, cm	0.2 (0-1.2)
SUVmax	0.9 (0-9.8)
Clinical T descriptor	
1a	155 (64.9)
1b	84 (35.1)
Procedure	
Lobectomy	90 (37.7)
Segmentectomy	56 (23.4)
Wedge resection	93 (38.9)
Positive invasion	
Lymphatic	3 (1.3)
Vascular	2 (0.8)
Pleural	1 (0.4)
Positive lymph node metastasis	2 (0.8)

Data are presented as median (range) or No. (%). GGO = ground glass opacity; SUVmax = maximum standardized uptake value.

Table 2—*Distribution of Operative Procedures in Patients With GGO-Dominant Clinical T1a and T1b Lung Adenocarcinoma*

Procedure	T1a Tumor (n = 155)	T1b Tumor (n = 84)	*P* Value
Wedge resection	79 (50.9)	14 (16.7)	...
Segmentectomy	37 (23.9)	19 (22.6)	< .001
Lobectomy	39 (25.2)	51 (60.7)	...

Data are presented as No. (%). See Table 1 legend for expansion of abbreviation.

There was no significant difference in 3-year RFS among patients with GGO-dominant tumors who underwent lobectomy (96.4%), segmentectomy (96.1%), and wedge resection (98.7%, $P = .44$) (Fig 1A). Three-year OS also was not significantly different among patients with GGO-dominant tumors who underwent lobectomy (97.6%), segmentectomy (98.2%), and wedge resection (98.7%, $P = .66$) (Fig 1B).

There was no difference in pathologic invasiveness, including lymphatic, vascular, or pleural, between patients with T1a GGO-dominant tumors and those with T1b tumors (Table 4). For patients with T1b GGO-dominant tumors, there was no significant difference in 3-year RFS among those who underwent lobectomy (93.7%), segmentectomy (92.9%), and wedge resection (100%, $P = .66$) (Fig 1C). Likewise, there was no difference in 3-year OS among patients with T1b GGO-dominant tumors who underwent lobectomy (95.9%), segmentectomy (100%), and wedge resection (100%, $P = .56$) (Fig 1D).

A multivariate Cox proportional hazards model for RFS included the preoperative variables of age, sex, clinical T descriptor, solid tumor size, SUVmax, and surgical procedure. However, none of these variables were independent prognostic factors (Table 5).

Discussion

The results of this study showed that patients with GGO-dominant clinical stage IA lung adenocarcinomas rarely had pathologically invasive tumors and had an excellent prognosis. These findings were consistent with previous reports showing that GGO-dominant lung adenocarcinoma had low malignant potential and good prognosis.[6,7] In addition, the current study showed that 3-year RFS and OS after sublobar resection were similar to those after lobectomy, without significant differences in GGO-dominant clinical stage IA lung adenocarcinoma.

Table 3—*Recurrences in Patients With GGO-Dominant Tumors*

Patient	Age, y	Sex	Whole Tumor Size, cm	Solid Tumor Size, cm	SUVmax	Procedure	ly	v	pl	n	Recurrence Site	Outcome
1	82	M	2.6	1.0	1.5	Segmentectomy	0	0	0	0	Peritoneum	25 mo, alive
2	61	F	3.0	1.2	1.8	Lobectomy	0	0	0	0	Brain	67 mo, alive

F = female; ly = lymphatic invasion; M = male; n = lymph node metastasis; pl = pleural invasion; v = vascular invasion. See Table 1 legend for expansion of other abbreviations.

Sublobar resection generally is indicated for a small lung cancer, such as those ≤ 2 cm.[3,18,19] However, in the current study, GGO-dominant T1b tumors rarely showed pathologic invasiveness or lymph node metastasis. Moreover, there were no differences in 3-year RFS and OS between patients with GGO-dominant

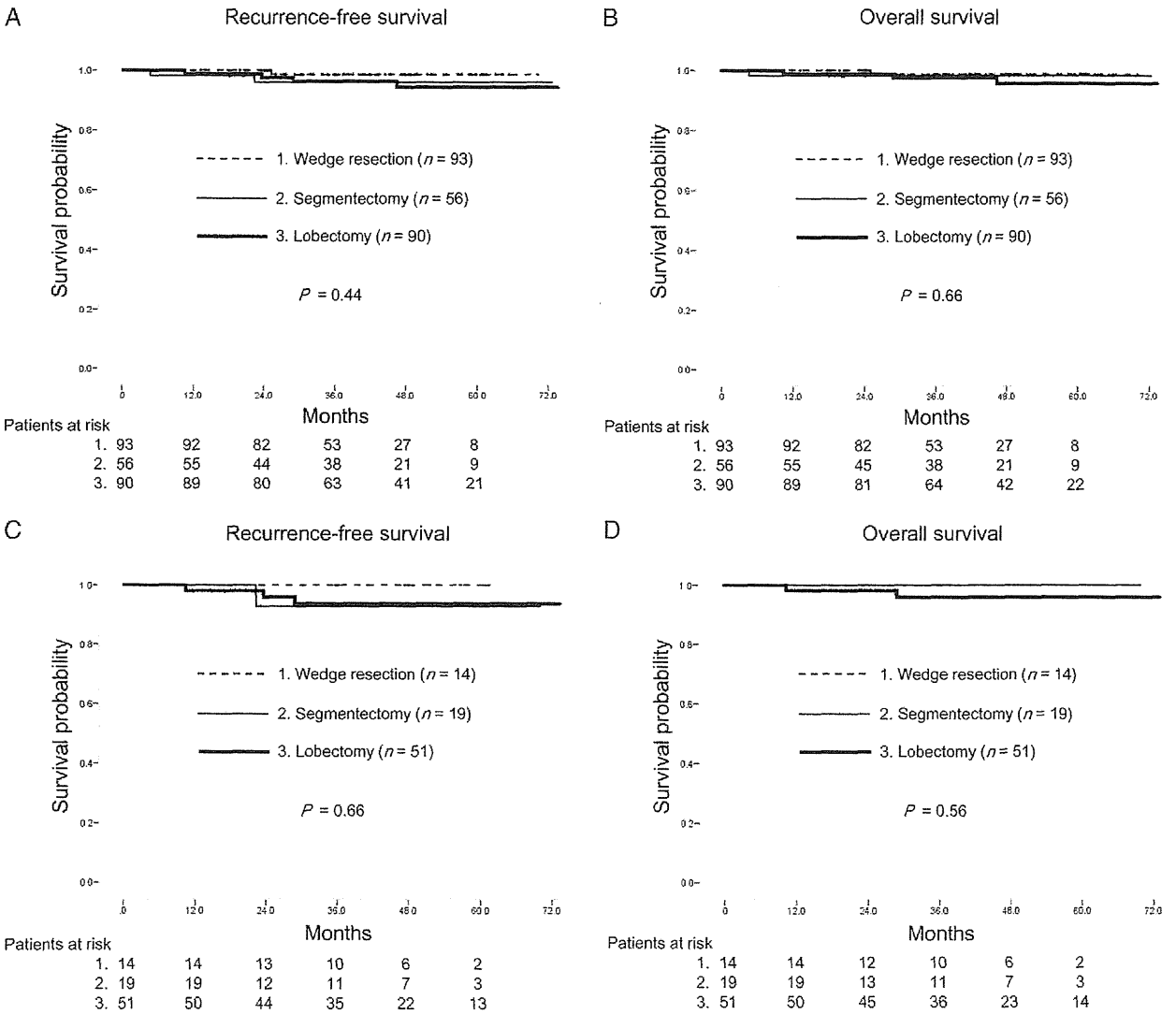

FIGURE 1. Recurrence-free survival (RFS) and overall survival (OS) curves for patients with ground-glass opacity (GGO) tumors who underwent lobectomy and sublobar resection. A, Three-year RFS rate for patients with GGO-dominant tumors who underwent wedge resection (98.7%; mean RFS, 69.8 mo; 95% CI, 68.6-70.9 mo), segmentectomy (96.1%; mean RFS, 70.3 mo; 95% CI, 67.3-73.4 mo), and lobectomy (96.4%; mean RFS, 71.4 mo; 95% CI, 61.9-73.7 mo; $P = .44$). B, Three-year OS rate for patients with GGO-dominant tumors who underwent wedge resection (98.7%; mean OS, 69.8 mo; 95% CI, 68.6-70.6 mo), segmentectomy (98.2%; mean OS, 71.4 mo; 95% CI, 69.0-73.7 mo), and lobectomy (97.6%; mean OS, 72.0 mo; 95% CI, 70.0-74.0 mo; $P = .66$). C, Three-year RFS rate for patients with GGO-dominant T1b tumors who underwent wedge resection (100%; mean RFS, not determined), segmentectomy (92.9%; mean RFS, 66.7 mo; 95% CI, 60.3-73.1 mo), and lobectomy (93.7%; mean RFS, 70.3 mo; 95% CI, 66.7-73.9 mo; $P = .66$). D, Three-year OS rate for patients with GGO-dominant T1b tumors who underwent wedge resection (100%; mean OS, not determined), segmentectomy (100%; mean OS, not determined), and lobectomy (95.9%; mean OS, 71.3 mo; 95% CI, 68.3-74.3 mo; $P = .56$).

Table 4—*Pathologic Findings for GGO-Dominant T1a and T1b Tumors*

Variable	T1a Tumors (n = 155)	T1b Tumors (n = 84)	*P* Value
Lymphatic invasion	1 (0.6)	2 (2.4)	.28
Vascular invasion	1 (0.6)	1 (1.2)	1.0
Pleural invasion	0 (0)	1 (1.2)	.35
Lymph node metastasis	0 (0)	2 (2.4)	.12

Data are presented as No. (%). See Table 1 legend for expansion of abbreviation.

T1b tumors who underwent lobectomy and those who underwent sublobar resection. Therefore, GGO-dominant T1b tumors could also be candidates for sublobar resection. We recommend segmentectomy and not wedge resection for sublobar resection of a GGO-dominant T1b tumor because these tumors could involve lymph node metastasis, and taking a sufficient surgical margin by wedge resection often is difficult in a T1b tumor.

In the current study, we found that two of 84 patients (2.4%) with GGO-dominant T1b tumors had lymph node metastases. No lymph node metastases were found for those with GGO-dominant T1a tumors. However, segmentectomy can approach hilar lymph nodes, whereas wedge resection cannot; thus, we should choose an optimal surgical procedure to avoid local recurrence in hilar lymph nodes, surgical stump, or residual lung. Segmentectomy would be superior to wedge resection for taking a sufficient surgical margin and for assessing hilar lymph nodes. Because sublobar resection includes both wedge resection and segmentectomy, it is necessary to distinguish between wedge resection and segmentectomy to clarify which procedure was used.

We encountered two distant recurrences with GGO-dominant T1b tumors: a brain metastasis after lobectomy and a peritoneal metastasis after segmentectomy, which could not be avoided even by standard lobectomy. One of the most important issues with sublobar resection is local control. Sublobar resection would be suitable for a GGO-dominant tumor because in this study, no intrathoracic local recurrence was observed, although a longer follow-up will be necessary before arriving at a definitive conclusion because of the indolent nature of GGO-dominant tumors.

Table 5—*Multivariate Analysis for Recurrence-Free Survival for Patients With GGO-Dominant Tumors*

Variable	HR (95% CI)	*P* Value
Age	1.08 (0.97-1.20)	.15
Male vs female sex	0.85 (0.18-3.91)	.83
T1b vs T1a descriptor	1.17 (0.20-6.70)	.86
Solid tumor size	6.37 (0.45-89.9)	.17
SUVmax	0.99 (0.52-1.90)	.99
Lobectomy vs sublobar resection	1.27 (0.20-7.93)	.82

HR = hazard ratio. See Table 1 legend for expansion of other abbreviations.

In the current study, the surgical procedure used and T descriptors were not independent prognostic factors of RFS in patients with GGO-dominant tumors, which also supports that a sublobar resection, such as a wedge resection or a segmentectomy, is suitable for GGO-dominant clinical stage IA lung adenocarcinomas, even for T1b tumors. In addition, solid tumor size and SUVmax were not independent prognostic factors of RFS. We previously reported that solid tumor size on HRCT scan and SUVmax on FDG-PET/CT scan were independent prognostic factors for lung adenocarcinoma.[14,20-22] However, patients with GGO-dominant lung adenocarcinomas have an excellent prognosis regardless of solid tumor size or SUVmax.

We speculate that GGO-dominant tumors indicate a uniform group exhibiting less tumor invasiveness and a favorable prognosis. In the current study, GGO-dominant tumors had small solid tumor sizes (median, 0.2 cm) and low SUVmax (median, 0.9). Prognosis based on solid tumor size and SUVmax may be useful, particularly for solid-dominant lung adenocarcinomas. In a previous study, we proposed N0 criteria that use a solid tumor size of < 0.8 cm or SUVmax of < 1.5 for predicting true N0 in clinical stage IA lung adenocarcinoma; patients who met these N0 criteria could be candidates for sublobar resection, such as wedge resection and segmentectomy.[11] Furthermore, patients with GGO-dominant tumors as well as those who meet the N0 criteria can be good candidates for wedge resection or segmentectomy.

Because this was a retrospective study, it is possible that patients who underwent sublobar resection were highly selective. Clinical trials comparing surgical results between lobectomy and sublobar resection (segmentectomy or wedge resection) for clinical T1aN0M0 NSCLC are currently being conducted by the Cancer and Leukemia Group B (CALGB 140503) and the Japan Clinical Oncology Group/West Japan Oncology Group (JCOG0802/WJOG4607L). These study results should indicate the significance of sublobar resection for small NSCLCs.[23] Regarding T1b tumors, a prospective study of segmentectomy for GGO-dominant tumors is warranted.

In conclusion, GGO-dominant clinical stage IA lung adenocarcinomas are a uniform group of tumors that exhibit low-grade malignancy and have a favorable prognosis. Patients with GGO-dominant tumors can be treated with wedge resection for T1a tumors and segmentectomy for T1b tumors.

ACKNOWLEDGMENTS

Author contributions: Drs Tsutani and Okada had full access to all the data in the study and take responsibility for the integrity of the data and the accuracy of the data analysis.